UNIVERSITÉ LAVAL

A Novel Wide-Area Control Strategy for Damping of Critical Frequency Oscillations via Modulation of Active Power Injections

Thèse

Ruichao Xie

Doctorat en génie électrique
Philosophiæ doctor (Ph. D.)

Québec, Canada

RÉSUMÉ

Cette thèse propose une nouvelle stratégie d'amortissement des oscillations de fréquence critiques par la modulation de l'injection rapide de puissances actives, qui ouvre la voie à l'utilisation d'actionneurs géographiquement dispersés, par exemple des ressources énergétiques distribuées (DERs), dans le contrôle des basses fréquences dynamique de l'angle du rotor du réseau électrique, qui comprend les oscillations interzones et les oscillations de fréquence transitoire. La méthode proposée intègre ces deux dynamiques différentes dans un cadre basé sur un système linéaire invariant dans le temps, dans lequel le contrôle de l'oscillation de fréquence transitoire est traduit en contrôle de la dynamique de mode commun du système. A cet effet, un examen attentif de la relation entre la variation transitoire de fréquence et la dynamique du mode commun est effectué; Les simulations montrent que le mode commun définit la forme d'un changement transitoire de faible signal de fréquence. La méthode de contrôle proposée vise à utiliser efficacement la réserve de marche limitée des DERs existants pour atténuer ces oscillations. Ceci est réalisé en découplant les actions de commande d'amortissement à différents endroits en utilisant les signaux d'oscillation du mode concerné comme commandes de puissance. Une base théorique pour cette commande de modulation découplée est fournie. Techniquement, les signaux d'oscillation modale souhaités sont filtrés en combinant linéairement les fréquences de l'ensemble du système, ce qui est déterminé par la technique (LQRSP). Avec la stratégie proposée, la modulation de chaque injection de puissance active peut être conçue efficacement en tenant compte de la limite de réponse et de la capacité de sortie en régime permanent du dispositif de support. Dans le cadre proposé, le signal de commande pour la commande de fréquence primaire est automatiquement déterminé dans une direction de commande (presque) optimale; des expériences montrent que ce signal a tendance à être la vitesse du système vue par le point d'injection de puissance. La commande modulante découplée a tendance à isoler les actions de commande pour les oscillations interzones et les oscillations de fréquence transitoire, ce qui atténue grandement les préoccupations concernant l'interaction entre la commande de ces deux types de dynamiques.

ABSTRACT

This dissertation provides a novel wide-area control strategy for damping of critical frequency oscillations via modulation of fast active power injections, which paves the way for the utilization of large-scale geographically dispersed actuators, e.g., distributed energy resources (DERs), in the control of power system low-frequency rotor angle dynamics, this includes the inter-area oscillations and the transient frequency swing. The proposed method incorporates these two different dynamics into a linear time invariant (LTI) system based control framework, in which the control of the transient frequency swing is translated into the control of the system common mode dynamics. For this purpose, a careful examination of the relationship between the transient frequency swing and the common mode dynamics is carried out; extensive simulations show that the common mode defines the shape of a small-signal transient frequency swing. The proposed control method pursues an efficient utilization of the limited power reserve of existing DERs to mitigate these oscillations. This is accomplished by decoupling the damping control actions at different sites using the oscillation signals of the concerned mode as the power commands. A theoretical basis for this decoupled modulating control is provided. Technically, the desired sole modal oscillation signals are filtered out by linearly combining the system-wide frequencies, which is determined by the linear quadratic regulator based sparsity-promoting (LQRSP) technique. With the proposed strategy, the modulation of each active power injection can be effectively engineered considering the response limit and steady-state output capability of the supporting device. In the proposed control framework, the power command signal for the primary frequency control is determined in a (near) optimal control sense; experiments show that this signal tends to be the system speed seen by the power injection point. Importantly, the decoupled modulating control tends to isolate the control actions for the inter-area oscillations and the transient frequency swing, thereby greatly relieving the concern about the interaction between the control of these two types of dynamics.

TABLE OF CONTENTS

LIST OF FIGURES

LIST OF TABLES

LIST OF PUBLICATIONS

R. C. Xie, I. Kamwa, D. Rimorov, and A. Moeini, "Fundamental study of common mode small-signal frequency oscillations in power systems," *International Journal of Electrical Power and Energy Systems*, vol. 106, pp. 201–209, Mar. 2019.

R. C. Xie, I. Kamwa, and C. Y. Chung, " A novel wide-area control strategy for damping of critical frequency oscillations via modulation of active power injections," *IEEE Transactions on Power Systems*, vol. 36, no. 1, pp. 485–494, Jan. 2021.

DEDICATION

For my parents

ACKNOWLEDGMENTS

I wish to thank my supervisor, Dr. Innocent Kamwa. His guidance, helpful discussions, and constructive criticism throughout my studies have been extremely helpful. I wish to thank my supervisor Dr. Hoang Le-Huy for his guidance, suggestions, and help throughout my studies. I wish to express my sincere appreciation to Dr. C. Y. Chung at the University of Saskatchewan for research supervision. I wish to thank Dr. Jérôme Cros for his invaluable support and encouragement. I wish to express my appreciation to Dr. André Desbiens, Mrs. Nancy Duchesneau, and Mr. Raoult Teukam Dabou for their invaluable help and support.

I wish to thank the smart lab members at the University of Saskatchewan for their help and insightful discussions during my visiting study.

I would also like to thank Dr. Dmitry Rimorov for many discussions related to power system dynamics.

FOREWORD

This dissertation is comprised of the contents presented in two published journal papers [A] and [B]. The goal of this work is to develop a control method that can handle large-scale geographically dispersed actuators for controlling power system low-frequency rotor angle dynamics. The paper [B], which presents the newly derived control method, is inserted in Chapter 2. The paper [A] is inserted in chapter 1; the study presented therein provides a strong support to incorporating the control of the transient frequency swing into a linear time invariant system based control framework, which is an essential basis for the proposed control method.

[A] R. C. Xie, I. Kamwa, D. Rimorov, and A. Moeini, "Fundamental study of common mode small-signal frequency oscillations in power systems," *International Journal of Electrical Power and Energy Systems*, vol. 106, pp. 201–209, Mar. 2019.

My author status: first author.

My role in preparing this article: Developed the approach; conducted simulations; wrote and revised the paper.

The role of co-authors in preparing this article: Provided important guidance and insightful suggestions.

[B] R. C. Xie, I. Kamwa, and C. Y. Chung, "A novel wide-area control strategy for damping of critical frequency oscillations via modulation of active power injections," *IEEE Transactions on Power Systems*, vol. 36, no. 1, pp. 485–494, Jan. 2021.

My author status: first author.

My role in preparing this article: Developed the approach; conducted simulations; wrote and revised the paper.

The role of co-authors in preparing this article: Provided important guidance and insightful suggestions.

INTRODUCTION

The Research Problem

The electric power industry is undergoing an unprecedented change in its energy structure. Driven by the primary goal of reducing the greenhouse gas emissions and increasing the system operational flexibility, many utilities are integrating electronically interfaced distributed energy resources (DERs), such as wind, solar and energy storage systems, into their transmission networks. Such an energy transition also brings new opportunities to the field of power system control. An emerging topic is the utilization of large-scale DERs in the control of the low-frequency rotor angle dynamics; this includes the inter-area oscillations and the transient frequency swing [12, 37-41]. The transient frequency swing is a process of the system converging to a new synchronous reference while the inter-area oscillations involve different groups of synchronous machines oscillate against each other around the system synchronous reference [61]. A sudden generation/load imbalance would significantly excite these two types of dynamics that threaten the reliability of the system operation. A real-life event is shown in Fig. I.1, which shows the devastating effect of such disturbances. The energy devices integrated using modern converters can usually provide the fast active power modulation capability; therefore, proper modulating actions may significantly improve the performance of the frequency dynamics due to the strong coupling of these two physical variables (i.e., active power vs. frequency) seen by the transmission system.

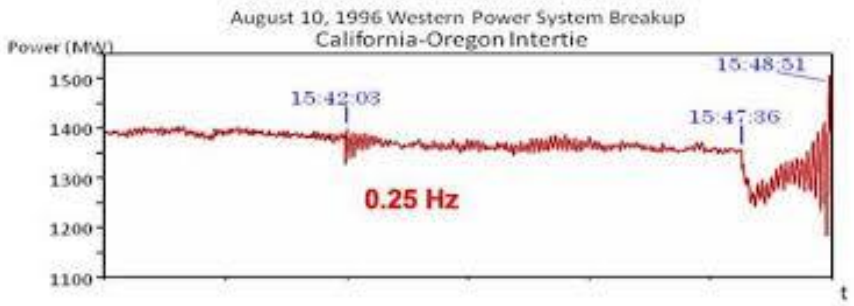

Figure I.1: 1996 western power system breakup: California-Oregon intertie.

Although promising, the DER-based damping control has been facing a fundamental challenge; that is, the power modulating actions must take into account the response limit and steady-state output capability of the supporting devices. Moreover, since the power devices are integrated for the consideration of economic operation, the headroom of individual devices for dynamic response may be small. As a result, it may need to take the efforts of many such devices to achieve a desired control effect. Intuitively, geographically dispersed actuators increase the controllability for the system-wide frequency oscillations while reducing the control burden at each single control site. However, in the context of classical dynamic and static feedback control, this may also significantly increase the computational burden brought about by the coordination of numerous controllers. To the best knowledge of the author, handling this problem with traditional control design is very difficult, especially when the amount of the controlled actuators is large. From the viewpoint of dynamics, the transient frequency swing is different from the inter-area oscillations. How to simultaneously mitigate them in a scientific way is never an easy task. Although many have used the linear method to analyze and control the transient frequency swing [3, 12, 19, 32], a control method that can effectively incorporate these two types of dynamics into a single framework is missing. In the context of the so-called grid following control, there is an ongoing research on the choice of command signals for the fast active power modulation based primary frequency control. Literature shows three directions in this line of research: using the system frequency as the power command signal to provide the so-called fast frequency response [39], using the derivative of the system frequency as the power command signal to provide the so-called virtual inertia [68], and a combination of them [12, 37]. How to effectively determine and manage the power command signals is still an open question.

This dissertation focuses on this so-called *multi-point active power modulation* problem and is devoted to developing a *wide-area control method* that can handle large-scale actuators while taking into account the above-mentioned challenges. From a broad point of view, the development of such a control method may also be useful for the utilization of other types of actuators in damping control.

Literature Review

Wide-Area Damping Control

The basic idea of wide-area damping control is using the remote measurements to drive the actuators such as synchronous machines, HVDC, dynamic loads, and DERs so as to achieve better control effect [63-64]. Taking the synchronous machines as an example, this section provides a general review of the damping control problem and highlights the advantage of the wide-area signals based damping control.

Modern power system typically involves power exchange between balancing areas. Consequently, poorly damped inter-area oscillations may occur, thereby limiting the capability of the power transfers. Under certain operating conditions, the inter-area mode may become lightly damped or even unstable. It is therefore desirable to take effective control actions to mitigate the oscillations. The damping control in power systems may be achieved via modulation of the excitation system of the synchronous machines [23]. The power system stabilizer (PSS), a dynamic feedback controller typically using the machine speed as input, drives the generator to induce a damping torque component on the turbine shaft so as to attenuate the machine speed deviations [23]. The modulation of excitation system has proved effective for mitigating the local oscillations; however, for the inter-area oscillations that involve energy exchange between different groups of synchronous machines, the decentralized damping control is usually less effective. Moreover, the $\omega \rightarrow V_{ref}$ feedback control loop is usually more sensitive to the generator's local mode; as a result, a zero of the open-loop system transfer function may be located near the inter-area mode [51], thereby limiting the movement of the inter-area mode in the complex plane under power system stabilizer (PSS) actions. To overcome this issue, PSS4B (a multi-band PSS) [32] to limit the movement of the local mode or filter PSS (FPSS) [42] to make the PSS focus on the inter-area mode may be required. When considerable PSSs are tuned to achieve a better damping control effect on both the local and the inter-area modes of oscillations of a large power system, the coordination of multiple dynamic feedback controllers is not a trivial task [32]. After several decades of development, the phasor measurement unit (PMU) has been widely deployed in the North American power grids as depicted in Fig. I.2. This allows the local controllers access remote measurements [32]. Importantly, the wide-area signals may help

constitute a decentralized/hierarchical control strategy, which has proved more effective than the decentralized control [32].

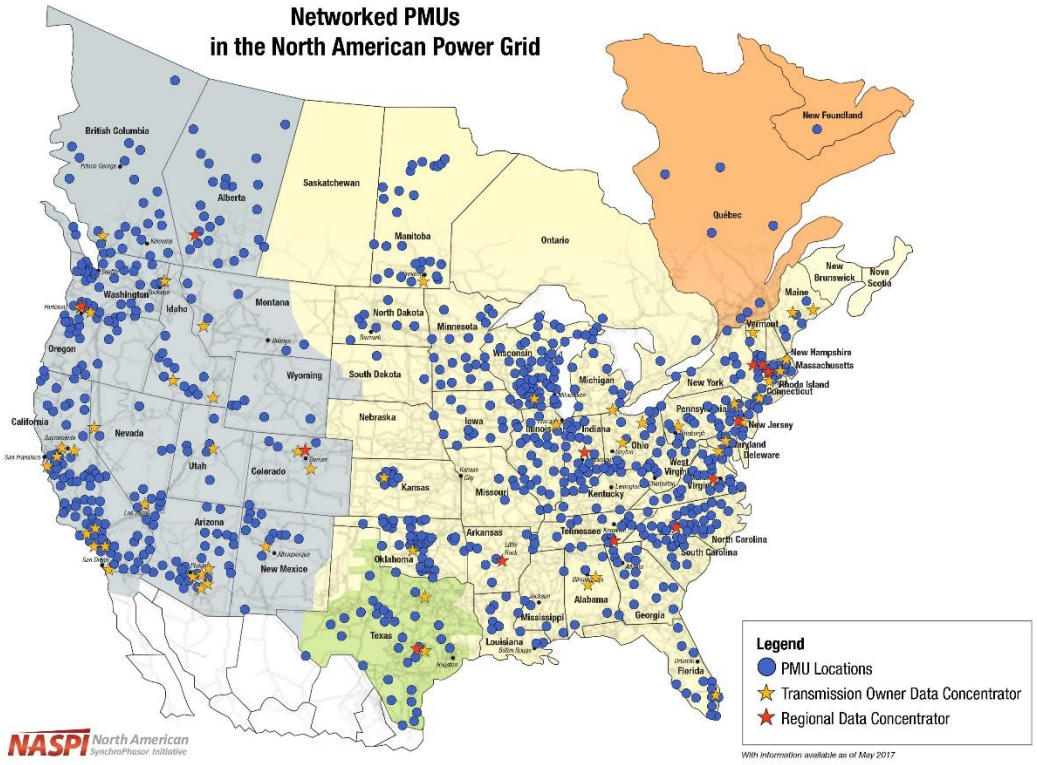

Figure I.2: Deployment of phasor measurement units in the North American power grid (credit: NASPI [70]).

Traditionally, for the damping control of inter-area modes, the actuators that execute the control actions usually need to be determined in the first place, as the inter-area modes are usually controllable at certain locations. Many small-signal analysis tools may achieve this: 1). Using eigen-decomposition of the state-space model of a power system to obtain the distributions of the controllability and observability or the residues matrix [23]; 2). Obtaining the above measures via impulse response based system identification [51]. Such approaches may be effective for the evaluation of the same type of actuators; however, when different types of actuators and feedback signals need to be determined, the eigenvector index may have scaling problem. In this regard, the geometric measure has proved more general and effective [32]. This measure is especially useful for selecting remote feedback signals to increase the controller's controllability. For example, the tie-line powers or currents may carry more rotor dynamics information than the bus frequency in some cases [52]. Although

the conventional modal indexes offer insight into the wide-area damping control design in terms of selecting the actuators and the feedback signals, they may not be able to guarantee the selected actuators to be sufficient in constituting an efficient control structure, in which a variety of local and remote system outputs may be employed [32]. Once the actuators and the feedback signals are determined, damping controllers can be designed. For a single actuator based damping control, the classic root-locus technique may be used to tune the controller parameters (gain and/or compensator time constants) [51]. If multiple controllers are involved, optimization process may be needed to coordinate the controllers in order to achieve a desired closed-loop system performance and the sequential control design may be employed [32]. In general, the control design is a computer-assisted work, and the basic process is setting a desired performance index as well as several constraints and solving for possible combinations of the controller parameters using optimization techniques. The performance index and constraints may be the H_2 and/or H_∞ index, eigenvalue index, saturation limits, and robustness considerations [32, 53-55].

Recently, taking advantage of the newly developed ADMM technique [71], a linear quadratic regulator based sparsity promoting (LQRSP) optimal control framework is established [44]. A salient feature of the approach is that it can identify a sparse control structure while optimizing the closed-loop system performance [45-46]. However, as will be explained in chapter 2 and Appendix, the control design method may not be applicable for the DER-based control.

Active Power Modulation Based Damping Control

Power system community has a long history of studying and practicing the active power modulation based damping control. An early attempt is the PDCI damping controller [48]. Because the DC line connects two oscillating areas, the modulating control showed significant effect on a major inter-area mode of the system. However, due to the restrictions on the choice of feedback signals, the controller was implemented with filtered local available measurements passing through a fine tuned compensator. Unluckily, unwanted control interactions appeared under certain operating conditions. With the advance of wide-area measurement system, recently it has been demonstrated that modulating the active power injection of a HVDC using the frequency difference of the DC line terminals (AC side) as

command signal to damp the critical inter-area oscillation of a large-scale power system is technically feasible [35-36]. However, the number of HVDC in a power system is usually limited; therefore, its ability to control multiple (concerned) inter-area modes is limited. Researchers have also been exploring the control of dynamic loads. The problem of stabilizing a bulk power system by modulating controllable active loads is investigated in [48-49]. However, the dynamic feedback control design may have scaling problem. An attempt to control of massive dynamic loads is presented in [69]; simulation results show that the distributed loads have great potential to enhance the dynamic performance of the system. The emergence of DERs brings new opportunities for the active power modulation based damping control. Unlike HVDC and dynamic loads, the DERs are independent power injection devices and may provide more flexible control functions without affecting the operation of the devices. A non-linear control strategy that coordinates the DERs for damping control is presented in [56]. The approach takes into account the input constraints; however, it may suffer from scaling problem when a large amount of DERs is controlled. An adaptive wide-area damping control for DER integrated power grid is proposed in [57]. Although this type of approaches may require less system model information, the robustness of the controller with respect to disturbances may not be guaranteed, as the location of the DERs are determined by many factors. Multiple models (or model bank) based adaptive damping control [64-66] which may be applied to DERs have been proposed as well, but their robustness during short-circuit faults close to the actuator locations is yet to be demonstrated. A so-called retrofit control method is presented in [58-59]. This method controls the DERs to mitigate the local disturbances; therefore, it may not be able to provide control effect if the disturbance location nearby has no DERs. The feasibility of applying model predictive control (MPC) as a viable strategy to damp the electromechanical oscillations is investigated in [60]. Although the MPC strategy is able to take into account the input constraints, the computational burden of the MPC approach may limit its applicability for dynamic control.

Given the nature of the DER-based control, major efforts toward the multi-point active power modulation based control for damping of the inter-area oscillations and the transient frequency swing are focused on coordinating the control actions using output feedback control strategies. By using the local frequency as the power command, a design method of

structurally constrained output feedback with bounded power responses is proposed in [37]; a non-linear simulation based optimization approach for coordinating the power modulations to damp the critical mode of oscillation is proposed in [38]; likewise, a gain tuning approach of load modulation for primary frequency regulation while considering the load's disutility is presented in [39]. The other method employs the system-wide frequencies to drive the active power modulations, a structurally constrained output feedback optimal control method is proposed in [40] for suppressing the inter-area oscillation of a two-area system; the approach is then further developed in [41] for controlling multiple inter-area modes while optionally improving the primary frequency response of a large-scale power system. All of these methods have distinct merits. Nevertheless, we note that the control performance of the local frequency based power modulation may be dependent on the system structure and the actuator location. We also note that although all the methods pursue an optimal coordination, the strategies may not be very cost-effective in terms of utilizing the valued active power response to resolve the oscillation issue, which is usually dictated by a couple of modes under an operating condition; moreover, the approaches are based on a centralized implementation (i.e., the modulations act as a single control action), which may yield a compromised control effect, and it is not easy to illustrate the role of each single-point control action in the oscillation damping.

Summary

The above literature survey demonstrates that achieving a high penetration of DERs to switching the economy to 100% renewable, gives rise to some major challenges in term of effectively controlling the frequency response of a system with lower inertia while ensuring adequate damping of inter-area oscillations in presence of millions of controllable agents. On one hand, we see an opportunity to use these massive DERs as so many control modulation sources that can be used to enhance the system stability without the need for additional investments. However, on the other hand, we face the challenge of an increased control complexity due to a large number of distributed actuators. Therefore, we consider that to maximize the grid hosting capability of DERs with respect to maintaining grid frequency response and dynamic stability, there are two main gaps that remain to be properly filled:

1). Since the inverter-based DERs are inertia-less generation, their large-scale adoption for decarbonizing the economy results inevitably in a deterioration of the frequency response of the power grid. Can we then use improved control techniques to enhance the frequency responses resulting from generation/load imbalances without deteriorating the performance of the electromechanical dynamics [67]? By strengthening the frequency response, such advanced controls based on the power modulation capability of existing assets may significantly increase the grid hosting capability of inertia-less DER.

2). Once the inverter-based DERs are massively integrated in the system without impeding the system frequency stability, thanks to the findings of the previous step, how can we leverage their active power modulation capability to enhance the overall stability of the power system with respect to the electromechanical oscillation more specifically? This is a huge challenge never addressed before, yet if successful, the DERs can become important flexible resources like smart loads, with the advantage of greater controllability thanks to their smart power electronics interface and larger total headroom available for safe and continuous action without influencing energy requirements on the grid users.

The aim of the research considered in this dissertation is to address the two research gaps identified above. We will first develop a mathematical and simulation based fundamental understanding of the common frequency oscillations in a power grid leading to identification of the underlying influencing factors. Building on this knowledge, we will develop a novel control method that has the ability to handle a large number of actuators, and effective in dealing with the two control objectives stated above.

The Research Work

This dissertation proposes a methodology that incorporates the transient frequency swing into a linear time invariant (LTI) system based control framework, which is usually employed for the design of electromechanical controls. In particular, the control of the transient frequency swing is translated into the control of the system common mode dynamics. To ascertain the feasibility of this substitution, the relationship between the common mode dynamics and the transient frequency swing is examined; this is presented in chapter 1 through an impact study of system components on the system frequency oscillations; simulation results clearly show that the common mode defines the shape of the transient frequency swing under relatively small disturbances. The proposed control method is presented in chapter 2. The method pursues an efficient utilization of the limited power reserve of existing DERs to mitigate the inter-area oscillations and the transient frequency swing. This is accomplished by decoupling the damping control actions at different sites using the oscillation signals of the concerned mode as the power commands. A theoretical basis for this decoupled modulating control is provided. Technically, the desired sole modal oscillation signals are filtered out by linearly combining the system-wide frequencies, which is determined by the linear quadratic regulator based sparsity-promoting (LQRSP) technique. With the proposed strategy, the modulation of each active power injection can be effectively engineered considering the response limit and steady-state output capability of the supporting device. In the proposed control framework, the power command signal for the primary frequency control is determined in a (near) optimal control sense; experiments show that this signal tends to be the system speed seen by the power injection point. Importantly, the decoupled modulating control tends to isolate the control actions for the inter-area oscillations and the transient frequency swing, thereby greatly relieving the concern about the interaction between the control of these two types of dynamics.

CHAPTER 1 SMALL-SIGNAL CHARACTERISTICS OF THE TRANSIENT FREQUENCY SWING

Inserted paper: R. C. Xie, I. Kamwa, D. Rimorov, and A. Moeini, "Fundamental study of common mode small-signal frequency oscillations in power systems," *International Journal of Electrical Power and Energy Systems*, vol. 106, pp. 201–209, Mar. 2019.

1.1 RÉSUMÉ

Ce chapitre présente une étude sur les caractéristiques des petits signaux de l'oscillation de fréquence transitoire. Les résultats montrent clairement que le mode commun définit la forme d'une fréquence transitoire sous des perturbations relativement faibles.

1.2 ABSTRACT

This chapter presents a study on the small-signal characteristics of the transient frequency swing. The results clearly show that the common mode defines the shape of a transient frequency under relatively small disturbances.

1.3 INTRODUCTION

In recent years, frequency oscillations associated with primary frequency response (PFR) occurred in several isolated power systems [1-3]. In fact, such oscillatory phenomena has been noticed long time ago, especially in hydro-dominated power systems, and their detrimental impact on the interconnection reliability were recognized very early [4]. The speed-governing system settings were shown to be the culprit of the oscillations [4-8], although their deadbeat performance tuning often masks the oscillatory phenomena in interconnected systems. Furthermore, several authors found that the frequency dynamics is governed by a so-called governor mode (termed common low-frequency mode in [8] and frequency-regulation mode in [9]). Further studies in [10] show that the change of system inertia and load voltage dependence can greatly alter the common mode stability. Moreover, the common mode is controllable via excitation voltage modulation by the so-called Multi-

Band PSS [8,10] or through blade pitching of type-3 wind turbine generator operating in a deloaded manner [9].

A damping torque analysis is performed in [3], which points out that the hydraulic turbine-governor transfer loop is easily creating negative damping torque at the common mode frequency and parameter optimization of the PID type governor is proposed to guarantee positive damping contribution from the turbine-governor in the very-low frequency range (say 0.01-0.1 Hz).

On the other hand, power system community has studied frequency response improvement intensively, especially since the emergence of large-scale renewables and NERC studies showing a 50% performance decline from 1994 to 2018. The synchronous condenser based reactive power modulation method is proposed in [11]. An approach for optimizing the participation of distributed energy resource in primary frequency response is proposed in [12]. A practical frequency control design for large scale of power system based on Multi-Band PSS is demonstrated in [13]. In essence, such approaches intend to improve the common mode damping in order to achieve improved frequency nadir.

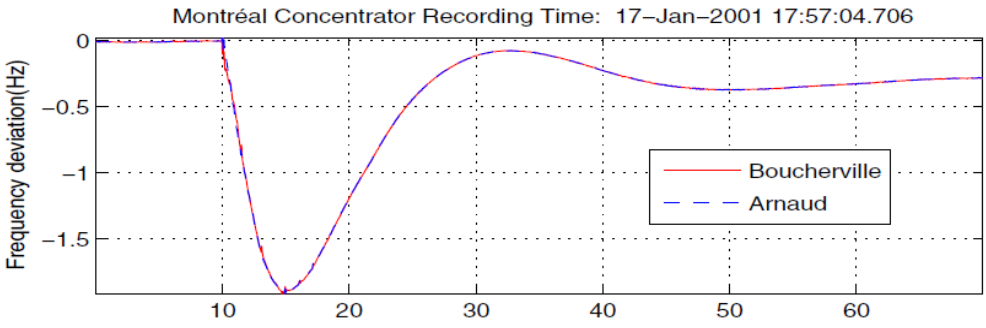

Figure 1.1: Large event in Hydro-Quebec system: loss of 3842 MW of generation. At 58.14-Hz frequency dip (5s later), 2700 MW load and 2148 Mvar capacitor were shed by the wide-area RAS

Despite above investigations using small-signal analysis tools to approach frequency response from an oscillation damping perspective, frequency stability is still defined in terms of "the ability of a power system to maintain steady frequency following a severe system upset resulting in a significant imbalance between generation and load" [14]. Therefore, the perception reinforced by the MW/0.1Hz NERC metric is that frequency stability is a large disturbance phenomenon. While a sufficient condition, it is not a necessary one [8,15].

Fig. 1.1 illustrates actual frequency response in Hydro-Quebec, following a large generation-load imbalance that results in frequency swings with a nadir performance of 3842MW/1.8Hz = 213MW/0.1Hz which is better than that specified by NERC [16]. The oscillation mode shape is the same at two substations separated by 1000km (Boucherville close to Montreal and Arnaud in the North-East). Fig. 1.2 illustrates the other facet of the frequency response, highlighting the devastating impact of poor damping. On the top of Fig. 1.2, spontaneous and sustained oscillations are observed, while on the bottom of the figure, an example of poorly damped very-low frequency oscillations triggered by 10% generation lost in the hydro-dominated system is given, the system generation is 7350MW in the first stage and 6700MW in the second stage, and clearly, as inertia decreases, the common mode becomes more unstable. These actual events show that while frequency instability is generally driven by large disturbances, poorly damped common mode due to inadequate acceleration power based PSS [8] or hydro-governor settings [3] is an aggravating factor and in some cases, an enabler of small-signal spontaneous unstable oscillations.

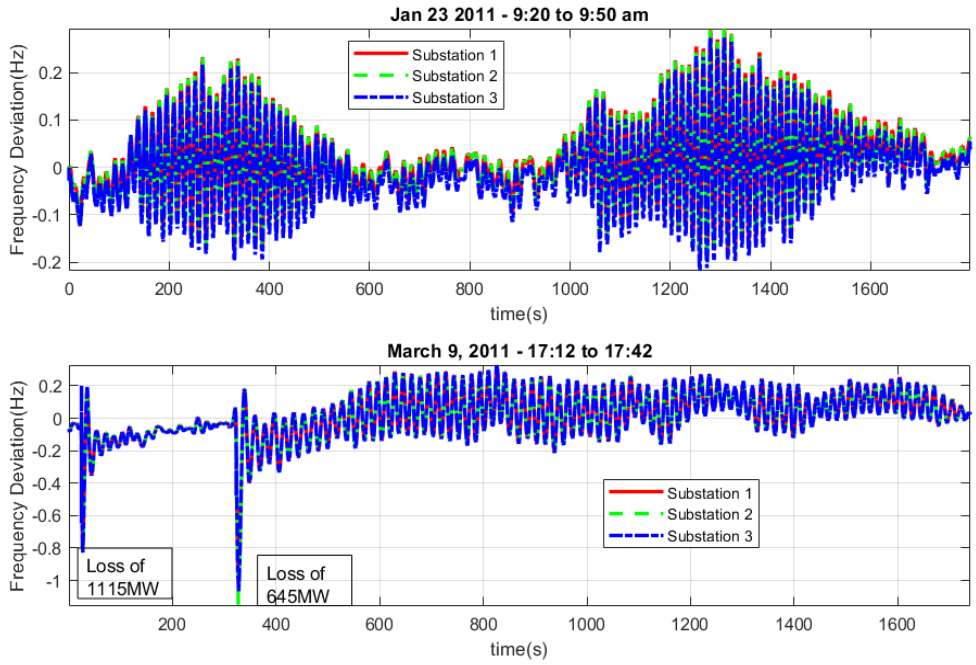

Figure 1.2: Unstable 0.05Hz-common mode oscillations in a Latin America interconnection with predominately hydro-generation.

As illustrated by these real-world examples, although the frequency dynamics has been recognized to be driven largely by the common mode, the fundamental nature of this mode

is still little explored, e.g., what factor influences most the frequency and damping of this mode in an interconnected system? The primary frequency control studies usually employ a single-machine equivalent model [17] by aggregating the turbine-governors, and use a load-damping term to represent the contribution of the frequency dependent load [12, 18-19]. However, as demonstrated in [10], the voltage dependent load may greatly affect the common mode dynamics, and its contribution is not necessarily just the damping.

Building upon existing studies, this chapter picks up the damping and synchronizing torque concept to investigate on a small parametric test system, the impact of turbine-governor type, load voltage sensitivity as well as system inertia on the common mode frequency oscillations. The findings are then confirmed on the New-England 39-bus test system. The main contributions are the following: (1) Using the damping-synchronizing torque concept to exhibit analytically for the first time in the literature the impact of several factors influencing the damping and natural frequency of the frequency oscillations in a multi-machine system. (2) Demonstrating for the first time the critical importance of small-signal modal analysis of frequency stability complemented with computed and/or measured damping and synchronizing torque coefficients in understanding and controlling frequency oscillations. (3) Revisiting the frequency stability definition by raising awareness on the understated role of common mode damping in primary frequency response, which exhibits large nadir and even becomes unstable under small load steps of 0.1% when the common mode is not well damped.

1.4 A DESCRIPTION OF THE FREQUENCY OSCILLATIONS

Because of the coherent mode shape property, by neglecting the transmission losses, the common mode frequency oscillation can be approximately described in per unit manner as [1,3,10]

$$2H\Delta\dot{\omega}(t) = \Delta P_G(t) - \Delta P_L(t) \tag{1.1}$$

where H is the equivalent inertia time constant, t is time, ω is the average speed of all synchronous generators or say system angular speed, P_G is the total active-power generation, P_L is the total active-power consumption, and Δ denotes the deviation from an (frequency) equilibrium. The frequency oscillations should not be confused with the electromechanical

oscillations that involve energy exchange between rotating masses. The system speed variation can be understood as the variation of the system synchronous reference, or say, the frequency oscillation is the process of system converges to new synchronous reference after breaking away from 60 Hz (for instance) triggered by the generation and load imbalance. Assuming that there are *m* generators and *n* loads responding to the system speed variation, (1.1) can be written,

$$2H\dot{\Delta\omega}(t) = \sum_{i=1}^{m} \Delta P_{G,i}\,(t) - \sum_{j=1}^{n} \Delta P_{L,j}(t) \tag{1.2}$$

Decomposing the power deviations w.r.t the new equilibrium as

$$\Delta P_{G,i}(t) = K_{D,i}\Delta\omega(t) + K_{S,i}\Delta\theta(t) \tag{1.3a}$$

$$\Delta P_{L,j}(t) = K_{D,j}\Delta\omega(t) + K_{S,j}\Delta\theta(t) \tag{1.3b}$$

and

$$\dot{\Delta\theta}(t) = \omega_s\Delta\omega(t) \tag{1.3c}$$

where ω_s is the system synchronous speed, $\omega_s \approx 1$ for the new synchronous speed after the generation-load imbalance event, and K_D and K_S are the damping and synchronizing torque coefficients, respectively. (1.2) can be rewritten,

$$\dot{\Delta\omega}(t) = \frac{\left(\sum_{i=1}^{m} K_{D,i} - \sum_{j=1}^{n} K_{D,j}\right)}{2H}\Delta\omega(t) + \frac{\left(\sum_{i=1}^{m} K_{S,i} - \sum_{j=1}^{n} K_{S,j}\right)}{2H}\Delta\theta(t) \tag{1.4}$$

Equations (1.3c) and (1.4) are actually representing the oscillatory dynamics of a single classical machine-infinity bus system, as long as the oscillation obeys (1.4), its damping factor and oscillation frequency can be determined by solving the state matrix of $\begin{bmatrix}\dot{\Delta\theta}\\ \dot{\Delta\omega}\end{bmatrix} = \begin{bmatrix}0 & \omega_s\\ \frac{\boldsymbol{K_S}}{2H} & \frac{\boldsymbol{K_D}}{2H}\end{bmatrix}\begin{bmatrix}\Delta\theta\\ \Delta\omega\end{bmatrix}$, where $\boldsymbol{K_D} = \sum_{i=1}^{m} K_{D,i} - \sum_{j=1}^{n} K_{D,j}$, and $\boldsymbol{K_S} = \sum_{i=1}^{m} K_{S,i} - \sum_{j=1}^{n} K_{S,j}$. The oscillation damping factor and the oscillation frequency can be given by,

$$\sigma = \frac{\boldsymbol{K_D}}{4H} \tag{1.5a}$$

$$f = \frac{1}{2\pi}\sqrt{\frac{-\omega_s \boldsymbol{K_S}}{2H} - \sigma^2} \tag{1.5b}$$

The oscillatory characteristics of the common mode is empirically formulated. In order to illustrate the factors that influencing the frequency oscillations, the approximate representation of the damping factor and oscillation frequency are further derived.

The formulation in (1.5) is based on the presented small-signal oscillation shape of the variables$\Delta P_{G,i}$,$\Delta P_{L,j}$ and$\Delta\omega$. For instance, by transforming (1.3a) and (1.3c) into the frequency domain, we have

$$\mathcal{F}\left[\Delta P_{G,i}(t)\right] = K_{D,i}\mathcal{F}[\Delta\omega(t)] - j\frac{\omega_s}{2\pi f}K_{S,i}\mathcal{F}[\Delta\omega(t)] \tag{1.6}$$

where $\mathcal{F}[\ \ ]$ denotes the Fourier transform. Without loss of generality, a single-mode oscillatory signal can be represented as $y(t) = \varphi_y B e^{\lambda t}$, where φ_y is a complex number defining the mode shape of variable y, B is scalar, and $\lambda = \sigma + j2\pi f$. Therefore, the damping and synchronizing torque coefficients can be given by

$$K_{D,i} = \mathrm{Re}\left\{\frac{\mathcal{F}\left[\Delta P_{G,i}(t)\right]}{\mathcal{F}[\Delta\omega(t)]}\right\} = \mathrm{Re}\left\{\frac{\varphi_{Gi}}{\varphi_\omega}\right\} \tag{1.7a}$$

$$K_{S,i} = -\frac{2\pi f}{\omega_s}\mathrm{Im}\left\{\frac{\mathcal{F}\left[\Delta P_{G,i}(t)\right]}{\mathcal{F}[\Delta\omega(t)]}\right\} = -\frac{2\pi f}{\omega_s}\mathrm{Im}\left\{\frac{\varphi_{Gi}}{\varphi_\omega}\right\} \tag{1.7b}$$

where Re and Im denote the real and imaginary part operators, respectively, φ_{Gi} and φ_ω represent the mode observability seen by the variables $\Delta P_{G,i}$ and $\Delta\omega$, respectively. For small σ, consider

$$\frac{\varphi_{Gi}}{\varphi_\omega} = \frac{\Delta P_{G,i}(\lambda)}{\Delta\omega(\lambda)} \approx \frac{\Delta P_{G,i}(j2\pi f)}{\Delta\omega(j2\pi f)} \tag{1.8a}$$

$$f \approx \frac{1}{2\pi}\sqrt{\frac{-\omega_s \boldsymbol{K_S}}{2H}} \tag{1.8b}$$

where $\Delta P_{G,i}(\lambda)/\Delta\omega(\lambda)$ denotes the output-to-output transfer function between the variables $\Delta P_{G,i}$ and $\Delta\omega$ evaluated at λ, and $\Delta P_{G,i}(j2\pi f)/\Delta\omega(j2\pi f)$ denotes the transfer function evaluated at $j2\pi f$ seen by the system input with considerable controllability for the mode.

The approximation in (8a) is widely used in the electromechanical mode shape estimation [20, 21] based on $\sigma \ll j2\pi f$. While such condition may not hold well for the common mode as the mode frequency is small (e.g., less than 0.1 Hz), the relation in (1.8a) is still adopted since the mode frequency lies in the range of 0.01-0.1 Hz which is distinguishable from the other rotor-speed modes. Using the approximations, the damping factor and oscillation frequency in (1.5) become

$$\sigma \approx \frac{\mathbf{1}}{4H}\left[\mathrm{Re}\left\{\sum_{i=1}^{m}\frac{\Delta P_{G,i}(j2\pi f)}{\Delta\omega(j2\pi f)} - \sum_{j=1}^{n}\frac{\Delta P_{L,j}(j2\pi f)}{\Delta\omega(j2\pi f)}\right\}\right] \tag{1.9a}$$

$$f \approx \frac{\mathbf{1}}{4\pi H}\left[\mathrm{Im}\left\{\sum_{i=1}^{m}\frac{\Delta P_{G,i}(j2\pi f)}{\Delta\omega(j2\pi f)} - \sum_{j=1}^{n}\frac{\Delta P_{L,j}(j2\pi f)}{\Delta\omega(j2\pi f)}\right\}\right] \tag{1.9b}$$

The above representation offers an insight for studying the impact of system components on the frequency oscillations. The integration of power source may bring in responsive speed-power transfer loop thereby affecting the common mode damping and frequency. The oscillation frequency tends to increase in presence of additional positive $\mathrm{Im}\left\{\frac{\Delta P_{G,i}(j2\pi f)}{\Delta\omega(j2\pi f)}\right\}$ or negative $\mathrm{Im}\left\{\frac{\Delta P_{L,j}(j2\pi f)}{\Delta\omega(j2\pi f)}\right\}$, and vice versa, consequently the oscillation frequency will define the damping torque, therefore the mode damping factor (oscillatory stability). It is interesting to note that, to some extent, (1.9a) and (1.9b) characterize the boundary of small-signal frequency stability, the approximation approaches equal as σ approaches 0. As will be shown later, the formulation is useful to illustrate the evolution of the small-signal frequency dynamics in the following simulation studies.

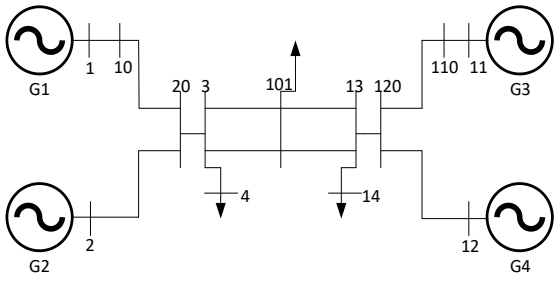

Figure 1.3: The modified four-machine test system.

1.5 FREQUENCY OSCILLATIONS IN A TEST SYSTEM

The simulations in this chapter are carried out using Power System Toolbox (PST) [22]. The two-area four-machine (Kundur's) system prototype [23] is modified for the study, as depicted in Fig. 1.3.

The generators are identical and modelled using a detailed sub-transient model. The inertia constant for each generator is 5. The same dc-exciter and conventional $\omega - V_{ref}$ PSS (without careful tuning) are installed on the generators. The transmission lines are modelled with loss. The ZIP (constant impedance, constant current, and constant power) load models are considered to mimic the load characteristics. A small load with 0.02 (per unit) active-power consumption is placed at bus 101 for the purpose of small-signal frequency response simulation. The active-power loads composition is listed in Table 1.1. The reactive-power loads are modelled as constant impedance. So far, all the simulation settings are as usual as the electromechanical dynamic stability simulation, asides from the turbine-governor. The generation and load power data are G1: P(5.7835), Q(1.015); G2: P(7.00), Q(0.9222); G3: P(5.16), Q(0.5915); G4: P(7.00), Q(0.1348); Load at bus 4: P(9.76), Q(1); Load at bus 14: P(14.63), Q(1); Load at bus 101: P(0.02).

Table 1.1: Load Composition: Constant Power Loads

	Constant P	Constant I	Constant Z
Bus 4	99%	1%	0
Bus 14	99%	1%	0
Bus 101	80%	0	20%

The system modes relevant to the rotor speeds are first calculated using ***Matlab*** linearization tool and shown in Table 1.2 (Case I). It is seen that the common mode does not appear, which indicates that the system will not undergo frequency excursion if the generation-load balance is broken. This is confirmed by rejecting the small load at bus 101, as shown in Fig. 1.4. In this paper, the small load rejection is used for all the frequency response simulations for the Kundur's system, the average of the synchronous machine speeds is used to capture the so-called "system speed". This is not in conflict with the center-of-inertia speed formula used elsewhere (e.g., [10]), as the inertia constant of the generators are the same for this test system. For unequal inertia constant case, the direct averaging will have a little lower ability in removing the inter-machine oscillations from the system speed trajectory.

Table 1.2: System Rotor-Speed Modes for Hydro-Dominated System

	Case I	Case II	Case III
Local I	-0.80+j8.02	-0.80+j8.01	-0.80+j8.00
Local II	-0.81+j7.93	-0.80+j7.92	-0.78+j7.90
Inter-area	-0.28+j4.13	-0.25+j4.10	-0.24+j4.10
Common	X	-0.022+j0.22	0.005+j0.32
	Case IV	Case V	Case VI
Local I	-0.79+j8.00	-0.77+j7.97	-0.77+j7.99
Local II	-0.79+j7.90	-0.78+j7.88	-0.77+j7.92
Inter-area	-0.22+j4.08	-0.20+j4.07	-0.10+j4.18
Common	0.034+j0.39	0.065+j0.45	-0.070+j0.39

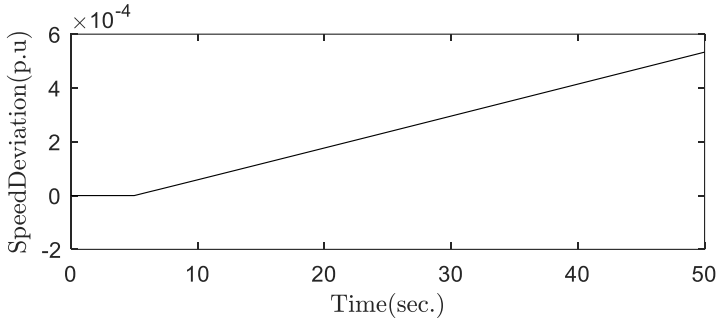

Figure 1.4: System speed for Case I: no turbine governor

1.5.1 IMPACT OF HYDRO-TURBINE SPEED-GOVERNING

Consider a turbine-governor (TG) model depicted in Fig. 1.5.

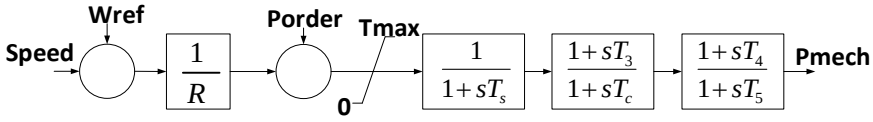

Figure 1.5: A simplified turbine-governor model.

Thus, the transfer function between the speed and mechanical power is defined,

$$\frac{\Delta P_m(s)}{\Delta\omega(s)} = -G_{tg}(s) = \frac{-(1+sT_3)(1+sT_4)}{R(1+sT_s)(1+sT_c)(1+sT_5)} \tag{1.10}$$

A set of parameters are selected for (1.10) to represent a hydro-type TG, as listed in Table 1.3.

Table 1.3: Parameters for A Hydro-Type TG

R	Ts	Tc	T3	T4	T5
0.05	0.5	10	1	-1	0.5

The TG model is enabled on generator 1, the system rotor-speed modes are recalculated, and listed in Table 1.2 (Case II). It is seen that the common mode appears and is stable. The small load rejection is simulated, and the system speed variation is shown in Fig. 1.6. As can be seen, the system converges to a new synchronous reference, albeit experiences oscillation. The oscillation frequency is 0.035 Hz indicating the common mode dynamics. Since the loads are almost constant power, it is expected that the common mode dynamics would be mainly governed by the mechanical power modulation in accordance with (1.2). For verification purpose, the exciter and PSS are removed, the common mode is -0.0286 + j0.2169.

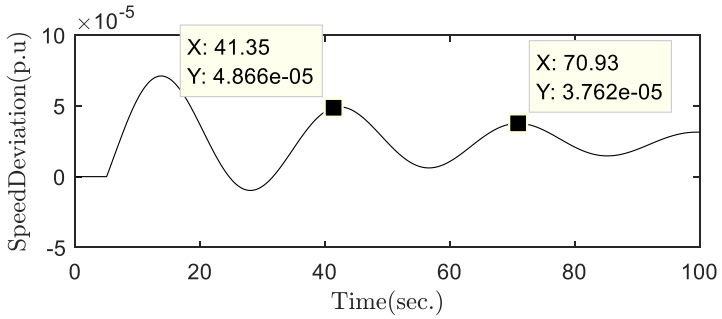

Figure 1.6: System speed for Case II. Single hydro-TG.

The Re$\{-G_{tg}(f)\}$ as well as Im$\{-G_{tg}(f)\}$ ($G_{tg}(f)$ denotes $G_{tg}(s)$ evaluated at $j2\pi f$) over a continuous range of frequencies are plotted in Fig. 1.7 (a) and (b), respectively. It is seen that at the common mode frequency, the Re$\{-G_{tg}(f)\}$ is a negative number, which means a positive damping support in accordance with (9a). The Im$\{-G_{tg}(0.035)\}$ is a positive number of a significant value. The common mode appears possibly because of this strong synchronizing torque support.

The same TG model is added on generator 2. The rotor-speed modes are altered (Table 1.2-Case III), especially the common mode becomes unstable. The small load rejection is simulated and the system speed variation is shown in Fig. 1.8. As can be seen,

the system failed to converge to a new synchronous reference. According to (9b), the oscillation frequency tends to increase on the basis of 0.035 Hz in the presence of additional $\mathrm{Im}\{-G_{tg}(0.035)\}$. However, even though the total number of $G_{tg}(f)$ is increased, the $G_{tg}(f)$ falls at 0.051 Hz, as marked in Fig. 1.7 (a), consequently results in an un-damped common mode.

The TG model is added on generator 3 and 4 in sequence, the system rotor-speed modes are listed in Table 1.2 under Case IV and Case V, respectively. The system frequency response for both cases are plotted in Fig. 1.9 (a) and (b), respectively. As observed in the former case, the common mode frequency becomes larger and larger; meanwhile the mode becomes more and more unstable.

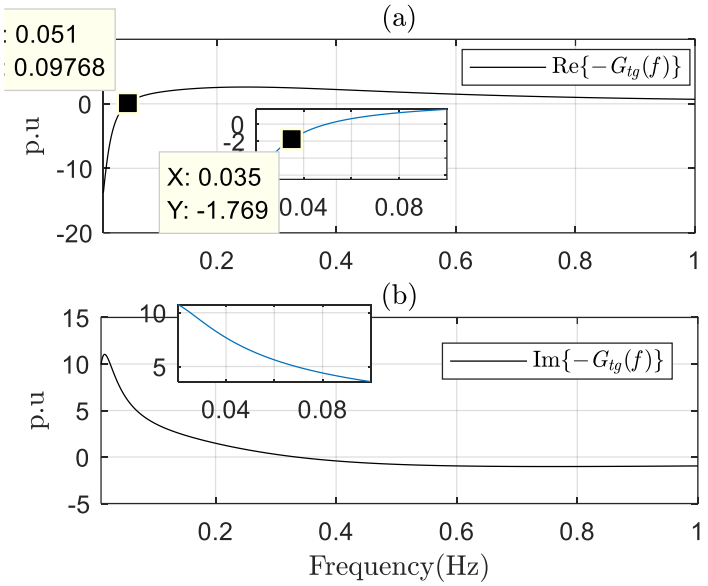

Figure 1.7: Real and imaginary parts for $-G_{tg}(f)$.

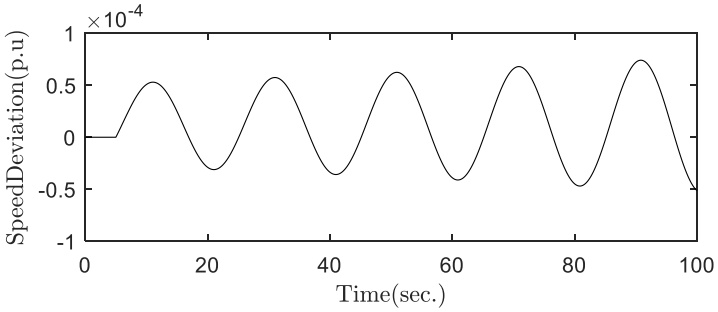

Figure 1.8: System speed for Case III. Two hydro-TGs.

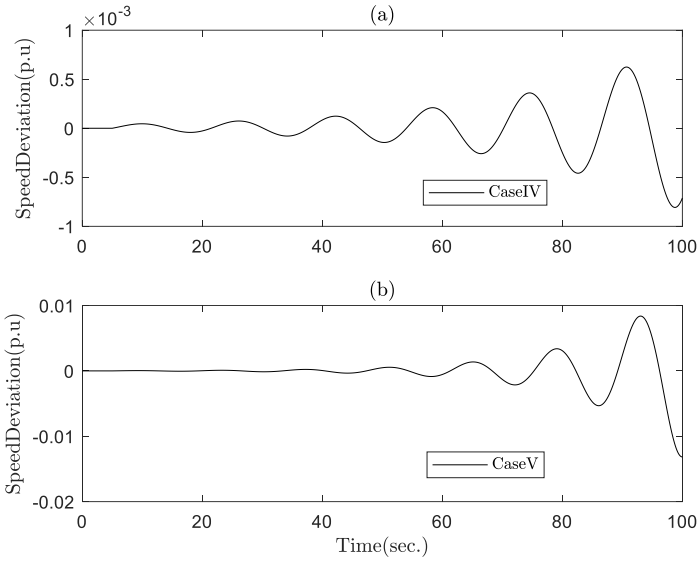

Figure 1.9: System speed for Case IV and Case V. Three and four hydro-TGs respectively.

It is noted that the inter-area mode damping is reduced. As can be seen in Fig. 1.7 (a), the TG has negative damping torque support around the inter-area mode frequency thus degrading the mode damping in accordance with the energy-flow theory in [24] and its frequency domain representation in [25]. The decrease of the inter-area mode frequency seems to be attributed to the TG's negative synchronizing torque support around the mode frequency.

1.5.2 IMPACT OF STEAM-TURBINE SPEED-GOVERNING

A set of parameters for (1.10) is considered to represent the turbine-governor as a steam-type, the parameters are listed in Table 1.4. The $\mathrm{Re}\{-G_{tg}(f)\}$ and $\mathrm{Im}\{-G_{tg}(f)\}$ over a continuous range of frequencies are plotted in Fig. 1.10 (a) and (b), respectively.

Table 1.4: Parameters for A Steam-Type TG

R	Ts	Tc	T3	T4	T5
0.05	0.5	10	3	0	0.05

Significant difference between the steam-type TG and the hydro-type TG is observed that is, in the very low frequency band (say below 0.1 Hz), the $\mathrm{Re}\{-G_{tg}(f)\}$ maintains negative. Enabling the TG model on generators by following the same procedure as done in the last sub-section. The system rotor-speed modes are calculated and listed in Table 1.5. It can be seen the common mode frequency increases as the $\mathrm{Im}\{-G_{tg}(f)\}$ adds in. Even though the larger mode frequency results in smaller individual $\mathrm{Re}\{-G_{tg}(f)\}$ (see Fig. 1.10 (a)), the increased total number of $\mathrm{Re}\{-G_{tg}(f)\}$ tends to accumulate a bigger damping factor for the mode. The frequency response for the four cases are plotted in Fig. 1.11. It clearly shows that the frequency response is much improved because of the damping characteristic of the steam-type TG. Moreover, more speed-governing results in smaller system speed bias from the original synchronous reference. However, this common grid-code may encounter difficulties when the hydro-type TG is dominant in the system (as observed in [1,4]), which can be inferred from the simulation studies in the last sub-section. On the other hand, the system is usually required to respond fast enough to compensate the power imbalance; this requires the common mode frequency should not be too small; again this requirement is unfavorable for the hydro-dominated system. As shown in [3], for the turbine equipped with PID-type governor, careful tuning of the PID parameters may guarantee the TG's damping contribution to the common mode under various loading conditions. Nevertheless, it remains to be seen if such settings are adequate in islanded conditions, which are the recommended scenario for validating governor settings [4].

For the steam TG scenario, the speed-governing has almost no influence on the inter-area mode damping, as the TG creates trivial damping torque around the mode frequency (see Fig. 1.10 (a)). It is true that the actual turbine-governor usually exhibits non-linearity, the impact of turbine-governor on the electro-mechanical oscillations may be complicated [26]. In addition, a strong adverse coupling between governor dynamics and low-frequency inter-area modes has been found in other studies [27] while acceleration power based PSS has been shown to influence the damping of the common mode adversely [8].

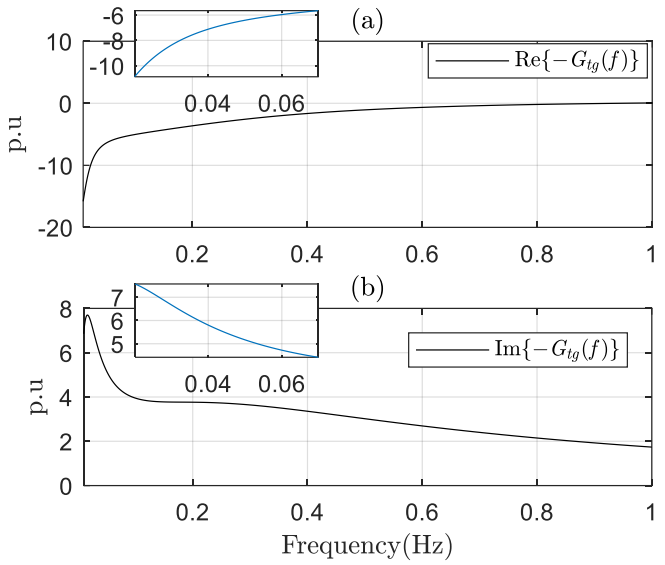

Figure 1.10: Real and imaginary parts for $-G_{tg}(f)$.

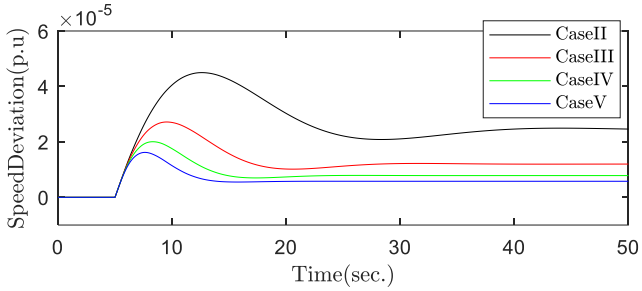

Figure 1.11: System speed for the steam TG scenarios. One, two, three and four steam TGs.

1.5.3 IMPACT OF LOAD VOLTAGE SENSITIVITY

Studies in [10] demonstrated that the load voltage sensitivity could play important role in shaping the common mode dynamics. Readers are also referred to [11] for the theoretical justification on the coupling of active power-speed and reactive power-voltage channels. The following analytical assessments aim to verify the conjecture and taking advantage of the disaggregation of the eigenvalue, where to enable and monitor the damping controls for the common and inter-area modes based on load voltage sensitivity are explained as well.

Table 1.5: System Rotor-Speed Modes for Steam-Dominated System

	No TG	Case II	Case III
Local I	-0.80+j8.02	-0.79+j8.04	-0.77+j8.07
Local II	-0.81+j7.93	-0.81+j7.95	-0.81+j7.96
Inter-area	-0.28+j4.13	-0.28+j4.18	-0.29+j4.21
Common	X	-0.11+j0.20	-0.19+j0.29
	Case IV	Case V	Case VI
Local I	-0.77+j8.08	-0.77+j8.10	-0.77+j8.11
Local II	-0.80+j7.99	-0.79+j8.00	-0.77+j8.04
Inter-area	-0.29+j4.25	-0.29+j4.27	-0.19+j4.36
Common	-0.29+j0.35	-0.45+j0.40	-0.98+j0.28

For the load composition in the previous cases, ΔP_L will be trivial during the speed variations. However, if we increase the percentage of constant impedance load in the load composition, the loads will significantly participate in the frequency response [10]. The modified load composition is listed in Table 1.6.

Table 1.6: Load Composition: Mixed Constant Power and Constant Impedance Loads

	Constant P	Constant I	Constant Z
Bus 4	50%	1%	49%
Bus 14	50%	1%	49%
Bus 101	80%	0	20%

The new load composition is enabled on the Case V in the hydro and steam TG scenarios, respectively. The system rotor-speed modes under this load model condition are listed in Table 1.2 and Table 1.5 under Case VI, respectively. The frequency response for the two cases are plotted in Fig. 1.12 (a) and (b), respectively.

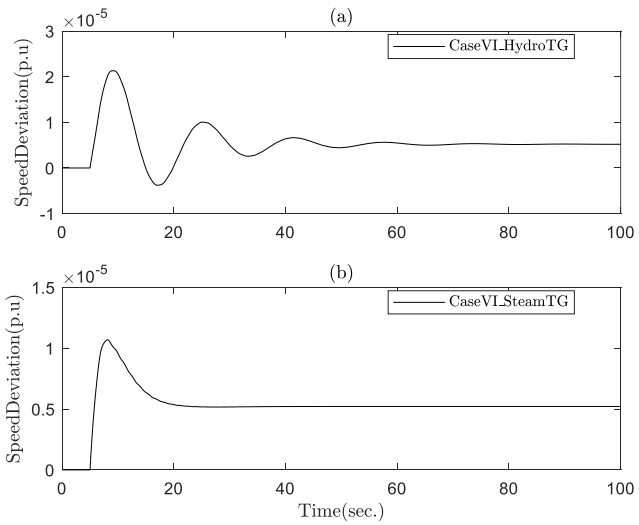

Figure 1.12: System speed for the new load composition scenarios.

An immediate observation is that the common mode frequency is reduced while its damping factor is much improved. However, for the hydro-TG scenario, the common mode frequency decreases to 0.062-Hz which still results in a negative damping torque support from the TGs (see Fig. 1.7 (a)). Therefore, there should be additional damping source present, to ascertain this, attention should be given to the load dynamics in accordance with (1.2). The polynomial load model for load *j* can be mathematically represented as

$$P_{L,j} = P_{L0,j}\left[a_1\left(\frac{V_{L,j}}{V_{L0,j}}\right)^2 + a_2\left(\frac{V_{L,j}}{V_{L0,j}}\right) + a_3\right] \tag{1.11}$$

where $V_{L,j}$ is the terminal voltage seen at the load-transmission interconnection point, $V_{L0,j}$ is the nominal voltage, $P_{L0,j}$ is the nominal active-power consumption of the load, and $a_1 + a_2 + a_3 = 1$. The linearization of (1.11) will define the small-signal dynamics of the voltage dependent load in a decoupled manner,

$$\Delta P_{L,j} = \frac{P_{L0,j}(2a_1 + a_2)}{V_{L0,j}}\Delta V_{L,j} \tag{1.12}$$

For a particular mode oscillation, decomposing the load power deviation with respect to the deviation of load bus speed $\Delta\omega_{L,j}$ as done in (1.3b) and (1.6), the damping and

synchronizing torque coefficients for the ZIP loads are

$$K_{D,j} = \mathrm{Re}\left\{\frac{\varphi_{V_{L,j}}}{\varphi_{\omega_{L,j}}}\right\}\frac{P_{L0,j}(2a_1 + a_2)}{V_{L0,j}} \tag{1.13a}$$

$$K_{S,j} = -\mathrm{Im}\left\{\frac{\varphi_{V_{L,j}}}{\varphi_{\omega_{L,j}}}\right\}\frac{2\pi f P_{L0,j}(2a_1 + a_2)}{\omega_s V_{L0,j}} \tag{1.13b}$$

where $\frac{\varphi_{V_{L,j}}}{\varphi_{\omega_{L,j}}}$ denotes the relative mode observability seen by the bus voltage and bus speed for load j. Denoting $G_{V_{L,j}\omega_{L,j}}(f) = \frac{\Delta V_{L,j}(j2\pi f)}{\Delta\omega_{L,j}(j2\pi f)}$, since the common mode governs all the bus frequencies oscillating coherently, according to (1.9a) and (1.9b), $G_{V_{L,j}\omega_{L,j}}(f)$ is examined to find out the participation of voltage dependent loads in the small-signal frequency dynamics. An ambient-condition simulation is carried out for the Case VI in the hydro-type TG scenario, a small percentage of load power are modelled as random, a 10-min data set is used for analysis, the $G_{V_L\omega_L}(f)$ for bus 14 is estimated using periodogram [28], and shown in Fig. 1.13. As a result, positive $\mathrm{Re}\{G_{V_L\omega_L}(f)\}$ in the very low frequency band is observed, which implies that the load tends to add damping to the common mode in accordance with (1.9a) and (1.13a); the positive $\mathrm{Im}\{G_{V_L\omega_L}(f)\}$ means that the additional synchronizing torque introduced by the load tends to reduce the mode frequency in accordance with (1.9b) and (1.13b). The bus 4 exhibits almost the same $G_{V_L\omega_L}(f)$ in the very low frequency band, thus not shown here.

An example is given to see how the transfer functions of the system components evaluated in the frequency domain reflect the eigenvalue solution. Considering equation (1.1) in the machine base (900 MVA), and considering the equivalent inertia $H = 4 \times 5 = 20$, according to Fig. 1.7 (a), at the common mode frequency, $\sum_{i=1}^{m}\frac{\Delta P_{G,i}(j2\pi f)}{\Delta\omega(j2\pi f)} = 0.7251 \times 4 = 2.9$, considering $V_{L0,j} \approx 1$(in the system base (100 MVA)), according to Fig. 1.13 (a) and eq. (13a), $\sum_{j=1}^{n}\frac{\Delta P_{L,j}(j2\pi f)}{\Delta\omega(j2\pi f)} = \big(3.5 \times 9.76 \times (2 \times 0.5)\big)/9 + \big(3.5 \times 14.63 \times (2 \times 0.5)\big)/9 = 9.5$, the damping factor given by (9a) is: $\sigma = \frac{2.9-9.5}{4\times 20} = -0.083$. According to Fig. 1.7 (b),

Fig. 1.13 (b), eq. (13b), and eq. (9b), $f \approx \left[5.484 \times 4 - \frac{(2.3\times9.76\times(2\times0.5))}{9} - \frac{(2.3\times14.63\times(2\times0.5))}{9}\right]/(20 \times 4\pi) = 0.06$. It is seen that the large voltage dependent load naturally has bigger influence on the common mode. It should be noted that the computation is found less accurate when the damping factor is large such as the Case V and VI in the steam-TG scenario. However, for the system, which is easily exhibiting oscillatory in the primary frequency response, the torque coefficient spectra of relevant components may be a convenient choice for quantitatively studying the performance of common frequency controls.

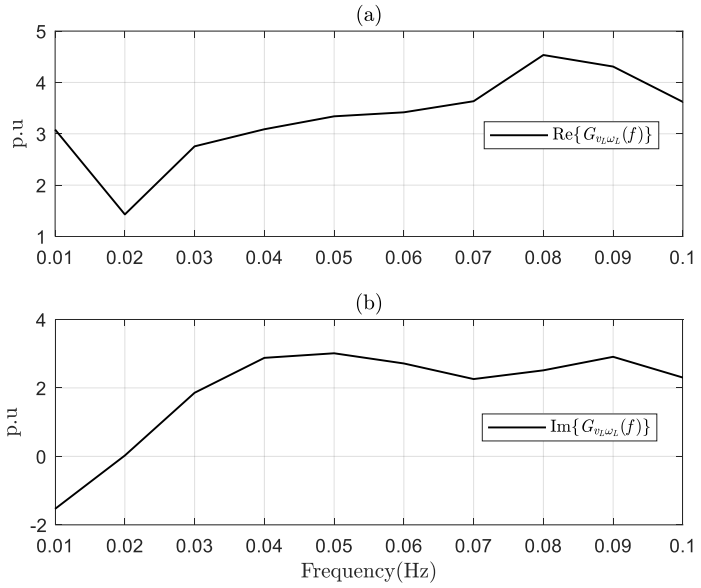

Figure 1.13: Real and imaginary parts for $G_{V_L\omega_L}(f)$ in the range of 0.01-0.1 Hz. Case VI with hydro-TGs.

To further verify that the speed-voltage coupling affects the common mode dynamics in the presence of voltage dependent load, two more cases on the basis of Case VI in the hydro-TG scenario are considered: (1). the PSS gain is tuned from 20 to 40, the common mode becomes -0.15+j0.29; (2). the PSS washout time constant is tuned from 5 to 1, the common mode becomes -0.02+j0.29. The Re$\{G_{V_L\omega_L}(f)\}$ and Im$\{G_{V_L\omega_L}(f)\}$ for bus 14 for the two cases are shown in Fig. 1.14 (a) and (b) respectively, it is seen that the variation of the speed-voltage relation dictated the change of common mode.

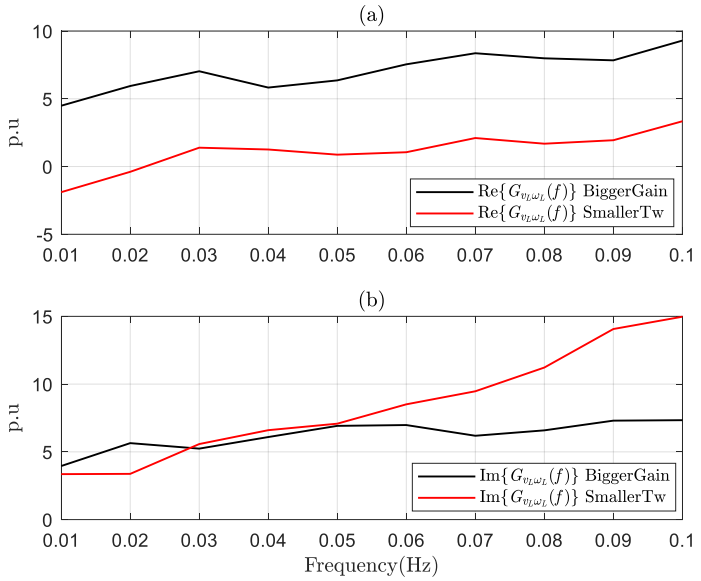

Figure 1.14: Real and imaginary parts for $G_{V_L\omega_L}(f)$ in the range of 0.01-0.1 Hz. Case VI with hydro-TGs (Bigger PSS gain and smaller washout time constant cases).

On the other hand, the impact of load voltage sensitivity on the common mode can also be viewed from the modal controllability (or say eigenvalue sensitivity for this mode) seen by the exciter voltage reference of the synchronous machines. As an example, for the Case V in the hydro-TG scenario, the common mode controllability seen by the exciter voltage reference of generator 4 is only 0.55, while for Case VI, the value jumps to 32.48, however, for generator 1, which is electrically further away from the largest load, the common mode controllability increases to 6.75 only.

Another observation from the Case VI in the hydro-TG scenario is that the inter-area mode damping is drastically reduced in the presence of voltage dependent loads. The reason is given as follows by leveraging the classical mode shape analysis [20] and an extended version of the energy-flow theory [24]. Considering the unit (4 generation units and 2 large loads) connected to each of the a.c. buses as rotating mass, using the ambient data set, the observability of the low frequency speed modes given by the estimated power spectral density (PSD) are shown in Fig. 1.15, as seen, the coherent peak at 0.06 Hz corresponds to the common mode, and the units at bus 11, 12, and 14 are much more observable for the inter-area mode, this is possibly because the system is sending power from the left-side to

the right side, considering the synchronous machine parameters are the same, the center-of-inertia is likely located on the left side of the system. The local modes are not observable in the spectra for this ambient dada set, possibly due to the high damping of the modes and/or the low controllability seen by the load power channels comparatively to the common and inter-area modes. The relative phase for the bus frequencies in the range of 0.1-1 Hz given by the estimated cross-power spectral density are shown in Fig. 1.16, it clearly shows that for the inter-area mode, the units at bus 1, 2, and 4 swing against with the units at bus 11, 12, and 14.

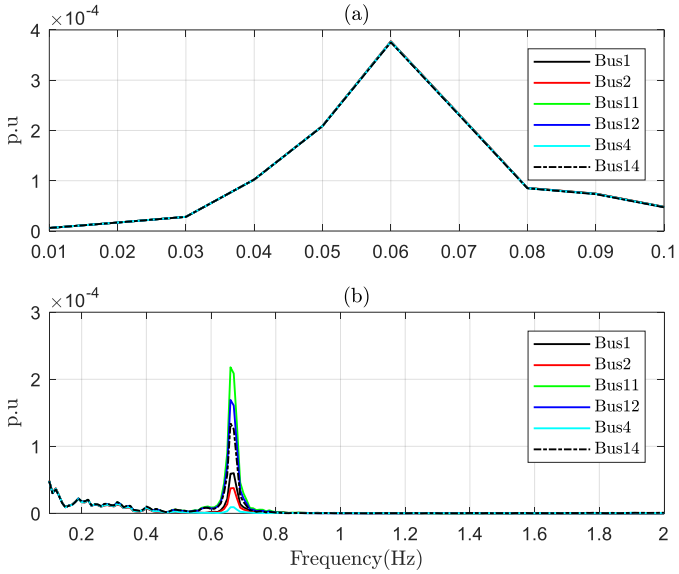

Figure 1.15: Estimated PSD spectra for the bus frequencies. Case VI for hydro-TGs.

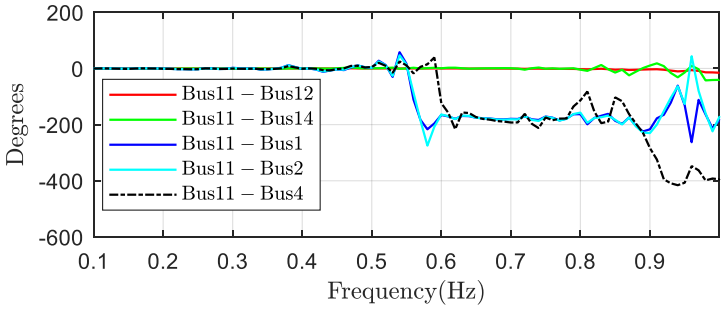

Figure 1.16: Estimated relative phase for the bus frequencies. Case VI for hydro-TGs.

The electromechanical mode damping factor is approximately inversely proportional to the total oscillation energy dissipation ability of the system components [24] because of the mode's small damping factor and fast oscillation frequency nature (the necessary

condition of this relation, see the derivation of eq. (1.27) in [24]), and the energy dissipation ability of the component connected to bus i is proportional to the product of the units damping torque coefficient and its squared speed denoted as $K_i \Delta\omega_i{}^2$ [25], therefore, the inter-area mode damping is more sensitive to the damping torque coefficient of the unit with larger observability for the mode. Checking the $G_{V_L\omega_L}(f)$ spectra in the electromechanical mode frequency range for bus 4 and bus 14, as shown in Fig. 1.17 (a), for bus 14, around the inter-area mode frequency, the $\mathrm{Re}\{G_{V_L\omega_L}(f)\}$ is negative, according to [24-25], the load is sending oscillation energy to the inter-area mode oscillation thus degrading the mode damping. Consider the load voltage dependence at bus 4 is shut down while the load voltage dependence at bus 14 is remained (50% constant Z), the inter-area mode changes from -0.1006+j4.1810 to -0.0863+j4.3641. However, if the load voltage dependence at bus 14 is shut down while keeping the load voltage dependence at bus 4 (50% constant Z), the inter-area mode changes from -0.1006+j4.1810 to -0.2279+j3.8353, which is close to the constant power case. It is clear that the inter-area mode damping is greatly enhanced by removing the bad damping contribution from the load at bus 14, however, the change in load at bus 4 does not alter the inter-area mode too much. Therefore, it can be reasonably inferred that for the reactive-power device nearby the key load area, its damping control function for the low frequency rotor-speed modes could be incorporated into the same framework.

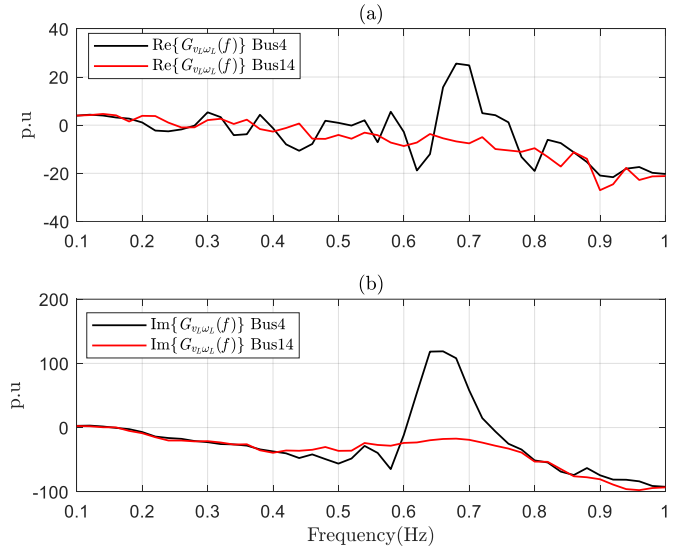

Figure 1.17: Real and imaginary parts for $G_{V_L\omega_L}(f)$ in the range of 0.1-1 Hz for bus 4 and bus 14 respectively. Case VI with hydro-TGs.

1.5.4 IMPACT OF SYSTEM INERTIA

It is demonstrated in [10] that the impact of system inertia on the common mode is hard to be generalized and tends to be case specific. However, for the hydro-dominated system, its frequency stability tends to be sensitive to the system inertia. Consider the Case V in the hydro-type TG scenario, the inertia constant of generator is gradually increased on the basis of 5 (uniform change of system inertia), as shown in Fig. 1.18 (a), the common mode frequency is gradually reduced, this could be explained by (1.9b). Importantly, this movement brings the mode to the left half plane. However, for the Case V in the steam-TG scenario, the increased inertia tends to reduce the mode stability, as shown in Fig. 1.18 (b), since larger inertia tends to lower the damping torque effort in accordance with (1.9a).

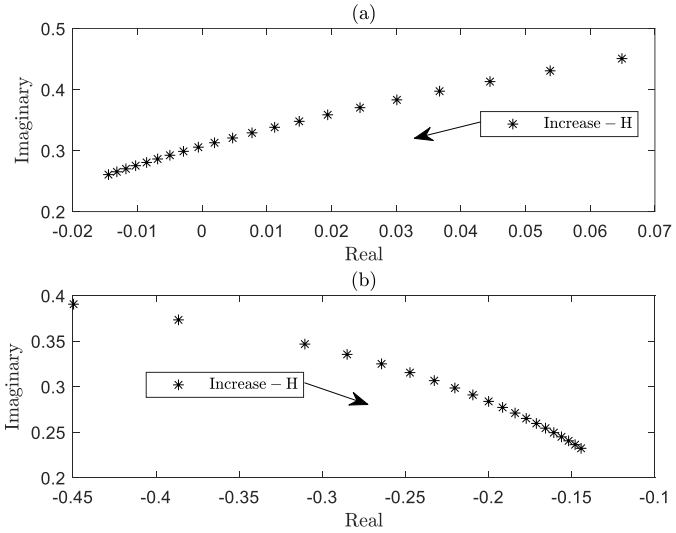

Figure 1.18: Common mode movement w.r.t the change of inertia (Kundur's system).

Therefore, loss of system inertia seems to be a potential threat to the frequency stability of a hydro-dominated power system. This fact is well documented in Quebec and Texas interconnections where solar and wind farms are now required to provide support for primary frequency response, especially during light load conditions [29]. As an example, consider the New-England 39-bus test system retrieved from [30]. The system consists of 10 generators and 19 loads; generator 1 is represented as an equivalent generation with inertia constant 50s. The hydro-TG model used in section 1.5.1 is enabled on generators 1-8, and the steam-TG model used in section 1.5.2 is enabled on generator 9. Some generators are equipped with PSS, all the active power loads are modelled as 80% constant Z plus 20%

constant P, and the reactive power loads are constant Z. The system's common mode given by linearization is -0.0403+j0.3489. Gradually decrease the inertia constant of generator 1 (no-uniform change of the system inertia), the common mode moves as shown in Fig, 1.19 (the dark star), the common mode for each of the four cases estimated by (1.9a) and (1.9b) is also plotted in the figure (the red circle), again, for small σ, the torque coefficients are capable of tracking the true eigenvalues indicating the effectiveness of the formulation. Two contingencies are considered, one is disconnecting generator 6, and the other is disconnecting generator 1. Both cases are simulated by disconnecting the tie lines of the generator and the system without faults. As shown in Fig. 1.20, the first contingency causes a converged frequency response, but the latter one results in a sustained (slightly grown) frequency oscillation in the system. This case study also indicates that the small-signal frequency stability may need to be considered as a constraint in system intentional islanding, since the common mode dynamics of the islanded systems will be triggered by the generation-load imbalance.

It is worth mentioning that the inertia emulation on non-synchronous power/energy sources may be a measure to prevent frequency oscillations in such systems, as the emulation is based on the formula [12]

$$\Delta P_{G,i}(t) = M\Delta\dot{\omega}_i(t) \tag{1.14}$$

where M is the emulated inertia, and is supposed to be a negative number. (1.14) can be transformed to the frequency domain,

$$\frac{\Delta P_{G,i}(j2\pi f)}{\Delta\omega_i(j2\pi f)} = j2\pi f M \tag{1.15}$$

According to the formulation, the emulated inertia tends to contribute negative synchronizing torque to the common mode (negative $\mathrm{Im}\left\{\frac{\Delta P_{G,i}(j2\pi f)}{\Delta\omega(j2\pi f)}\right\}$ in (1.9b)), therefore, can be used to keep the mode frequency in the low frequency range where the hydro-type

TGs guarantee positive damping to the common mode, hence the small-signal frequency stability of a hydro-dominated power system. Because of the modelling issue, the simulations considering inertia emulation are not conducted but the findings in [9] regarding blade pitching controller to support inertia and frequency response are consistent with our claims.

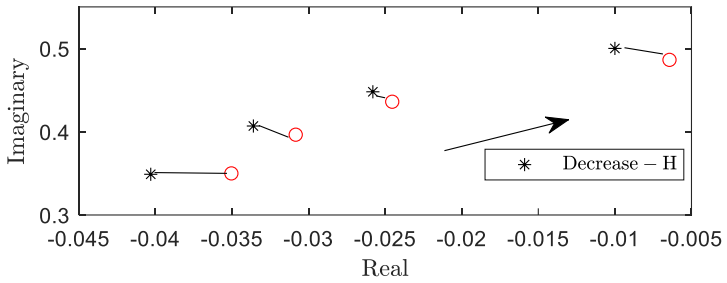

Figure 1.19: Common mode movement w.r.t the change of inertia. (New England 39-bus system)

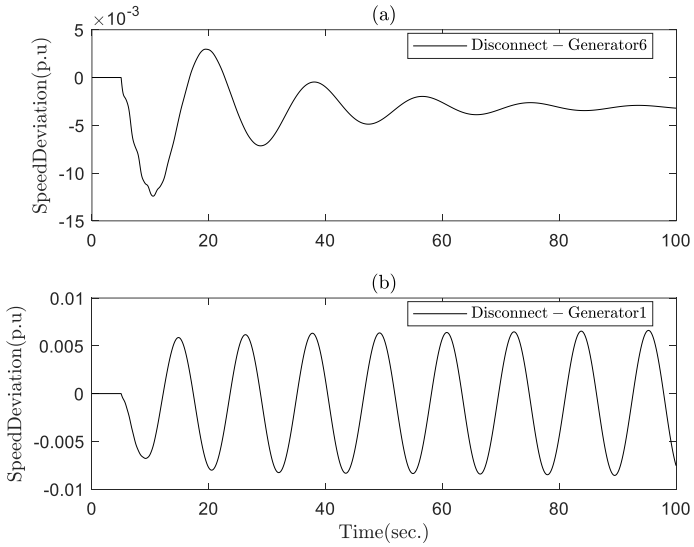

Figure 1.20: System speed for the New-England test system after outage of generator 6 and 1: Same regulation capacity, different inertias.

1.6 SUMMARY

The frequency oscillations in a test system are analyzed by leveraging the classical damping and synchronizing torque concept. The study clearly shows that the torque analysis is the proper tool for the study of small-signal frequency dynamics. Further simulations on

the 39-bus New England test system lends credibility to the findings on the 4-machine parametric test system, while actual recordings of common mode swings in hydro-dominant system confirms the strong relationship between the performance of primary frequency response and common mode oscillation damping. Comparative results show that the hydro-dominant power system is more easily subject to frequency oscillations. However, PID governor optimization, voltage modulation, inertia and/or damping emulation may be considered to mitigate frequency oscillations in such systems. Moreover, comparative results of the frequency and electro-mechanical oscillatory dynamics for the test system show the consistency of them in terms of damping and synchronizing torque properties. However, since the synchronism for the rotating masses is remained during the frequency oscillatory dynamics, it is suggested to term it the small-signal (oscillatory) frequency stability, in parallel with the frequency stability defined in [14]. In addition to the impact studies performed in the chapter, the other frequency responsive power sources, such as power electronic interfaced power/energy sources (e.g., battery energy storage system), and dynamic loads (e.g., induction motor), could be examined in the future by using the proposed analysis approach.

CHAPTER 2 A NOVEL WIDE-AREA CONTROL STRATEGY FOR DAMPING OF CRITICAL FREQUENCY OSCILLATIONS VIA MODULATION OF ACTIVE POWER INJECTIONS

Inserted paper: R. C. Xie, I. Kamwa, and C .Y. Chung, "A novel wide-area control strategy for damping of critical frequency oscillations via modulation of active power injections," *IEEE Transactions on Power Systems*, to be published, 2020.

2.1 RÉSUMÉ

Ce chapitre dérive une nouvelle stratégie de contrôle qui peut gérer un nombre illimité d'actionneurs. Son application à la modulation de puissance active multipoint est illustrée. La méthode de contrôle est validée sur la base d'un système à deux zones et des systèmes de 39 bus de la Nouvelle-Angleterre.

2.2 ABSTRACT

This chapter derives a new control strategy that can handle unlimited number of actuators. Its application to multi-point active power modulation is illustrated. The control method is validated based on a two-area system and the New-England 39-bus systems.

2.3 INTRODUCTION

Poorly damped inter-area oscillation modes limit the power transfer of a power system and may cause large-scale blackout. Traditional approaches for mitigation of these low-frequency oscillations include reducing the power flow of key transmission paths thru generation re-dispatch [31]; installing power system stabilizer (PSS) on synchronous machines [32] or supplementary damping controller on FACTS [33]. The common low-frequency mode or common mode (normally below 0.1 Hz) associated with the primary frequency response [32] may be lightly damped; consequently, under sudden imbalance in generation and load, large transient frequency and power swings and even sustained frequency and power oscillations may occur, this may trigger load rejection, critical line tripp

-ing, and subsequent cascading issues. Installing Multi-Band PSSs [32], retuning the PID-type speed governors [3] and disabling the speed governors [34] are effective measures in practice for mitigating such swings.

Recently, it has been demonstrated that modulating the active power injection of a HVDC to damp the critical inter-area oscillation of a large-scale power system is technically feasible [35-36]. As a matter of fact, with the proliferation of distributed energy resources (DERs), e.g., energy storage systems, active power modulation is becoming a cheap means of controlling the oscillatory dynamics of a power system.

Intuitively, geo-graphically dispersed actuators increase the controllability for the system-wide frequency oscillations while reducing the control burden at each single control site. However, in the context of classical feedback control, this may also significantly increase the computational burden brought about by the coordination of numerous controllers.

To date, major efforts toward the so-called multi-point active power modulation based damping control are focused on coordinating the control actions using output feedback control strategies. By using the local frequency as the power command, a design method of structurally constrained output feedback with bounded power responses is proposed in [37]; a non-linear simulation based optimization approach for coordinating the power modulations to damp the critical mode of oscillation is proposed in [38]; likewise, a gain tuning approach of load modulation for primary frequency regulation while considering the load's disutility is presented in [39]. The other method employs the system-wide frequencies to drive the active power modulations, a structurally constrained output feedback optimal control method is proposed in [40] for suppressing the inter-area oscillation of a two-area system; the approach is then further developed in [41] for controlling multiple inter-area modes while optionally improving the primary frequency response of a large-scale power system.

All of the above-mentioned methods have distinct merits. Nevertheless, we note that the control performance of the local frequency based power modulation may be dependent on the system structure and the actuator location. We also note that although all the methods pursue an optimal coordination, the strategies may not be very cost-effective in terms of utilizing the valued active power response to resolve the oscillation issue, which is usually dictated by a couple of modes under an operating condition; moreover, the approaches are based on a centralized implementation (i.e., the modulations act as a single control action),

which may yield a compromised control effect, and it is not easy to illustrate the role of each single-point control action in the oscillation damping.

A design concept of DER-based primary frequency control is presented in [12], where the authors employ a second-order linear model to superimpose the frequency controllers to achieve a desired damping ratio of the eigenvalue. Because the controllers are designed in a superposition manner, each power modulation can be conveniently engineered based on many considerations such as the response limit and steady-state output capability of the supporting device. Motivated by the result, this dissertation formulates a general wide-area control strategy for modulating the active power injections to damp the critical frequency oscillations in power systems; this includes the inter-area oscillations and the transient frequency swing.

2.4 STATIC MODAL DECOMPOSITION CONTROL

In [42], the modal decomposition control is introduced for PSS design. In this section, the concept is reviewed in the context of static feedback and therefore provides a basis for the control strategy to be proposed in the next section.

A power system can be described by a set of differential and algebraic equations, from which a single-input single-output (SISO) model may be obtained by linearizing the system around an operating point as follows:

$$\dot{\boldsymbol{x}} = \boldsymbol{A}\boldsymbol{x} + \boldsymbol{B}_i u_i \tag{2.1a}$$

$$y_i = \boldsymbol{C}_i \boldsymbol{x} \tag{2.1b}$$

where $\boldsymbol{x}$ is an $n \times 1$ state vector, $\boldsymbol{A}$ is an $n \times n$ state matrix, u_i is the input, y_i is the output, and $\boldsymbol{B}_i$ and $\boldsymbol{C}_i$ are the $n \times 1$ input and $1 \times n$ output vectors, respectively. The modal properties are given by $\boldsymbol{A}\boldsymbol{M} = \boldsymbol{M}\boldsymbol{\Lambda}$, $\boldsymbol{N}^T\boldsymbol{M} = \boldsymbol{I}$, where $\boldsymbol{M}$ and $\boldsymbol{N}$ represent the right and left modal matrices, respectively, $\boldsymbol{I}$ is an $n \times n$ identity matrix, and T denotes transpose. $\boldsymbol{M} = [\boldsymbol{m}_1, \boldsymbol{m}_2, \dots\dots, \boldsymbol{m}_n], \boldsymbol{N} = [\boldsymbol{n}_1, \boldsymbol{n}_2, \dots\dots, \boldsymbol{n}_n]$, where $\boldsymbol{m}_j$ and $\boldsymbol{n}_j$ are the $n \times 1$ right and left eigenvectors for mode j, respectively, and $\boldsymbol{\Lambda}$ is a diagonal matrix comprised of the system eigenvalues, denoted by $\boldsymbol{\Lambda} = \text{diag}(\lambda_1, \lambda_2, \dots\dots, \lambda_n)$.

Apply the linear transformation

$$\boldsymbol{x} = \boldsymbol{M}\boldsymbol{z} \tag{2.2}$$

where $\boldsymbol{z}$ is the state vector in the new coordinates. Then,

$$\dot{\boldsymbol{z}} = \boldsymbol{\Lambda}\boldsymbol{z} + \boldsymbol{N}^T\boldsymbol{B}_i u_i \tag{2.3a}$$

$$y_i = \boldsymbol{C}_i\boldsymbol{M}\boldsymbol{z} = \sum_{j=1}^{n} \boldsymbol{C}_i\,\boldsymbol{m}_j z_j \tag{2.3b}$$

where z_j is the j^{th} component of $\boldsymbol{z}$. Consider a sole modal signal scaled by a gain K as control input, denoted as

$$u_i = K\boldsymbol{C}_i\boldsymbol{m}_j z_j \tag{2.4}$$

The state equations then become

$$\dot{\boldsymbol{z}} = \boldsymbol{\Lambda}\boldsymbol{z} + \boldsymbol{N}^T\boldsymbol{B}_i K\boldsymbol{C}_i\boldsymbol{m}_j z_j = \boldsymbol{A}^*\boldsymbol{z} \tag{2.5}$$

where $\boldsymbol{A}^*$ is the closed-loop system state matrix in the new coordinates and

$$\boldsymbol{A}^* = \begin{bmatrix} \lambda_1 & 0 & \cdots & \boldsymbol{n}_1^T\boldsymbol{B}_i\,K\boldsymbol{C}_i\boldsymbol{m}_j & \cdots & 0 \\ 0 & \lambda_2 & \cdots & \boldsymbol{n}_2^T\boldsymbol{B}_i K\boldsymbol{C}_i\boldsymbol{m}_j & \cdots & 0 \\ \vdots & \vdots & \ddots & \vdots & \ddots & \vdots \\ 0 & 0 & \cdots & \lambda_j + \boldsymbol{n}_j^T\boldsymbol{B}_i K\boldsymbol{C}_i\boldsymbol{m}_j & \cdots & 0 \\ \vdots & \vdots & \cdots & \vdots & \ddots & 0 \\ 0 & 0 & \cdots & \boldsymbol{n}_n^T\boldsymbol{B}_i K\boldsymbol{C}_i\boldsymbol{m}_j & \cdots & \lambda_n \end{bmatrix} \tag{2.6}$$

The eigenvalues of the closed-loop system can be obtained by solving

$$\det(s\boldsymbol{I} - \boldsymbol{A}^*) = 0 \tag{2.7}$$

Equations (2.6) and (2.7) illustrate that the feedback control loop will only alter the j^{th} mode. Ideally, if $\boldsymbol{n}_j^T\boldsymbol{B}_i K\boldsymbol{C}_i\boldsymbol{m}_j$ is a negative real number, the j^{th} mode will be horizontally shifted to the left half plane without changing its frequency.

2.5 A STATIC MULTI-POINT CONTROL STRATEGY

Based on the theory in Section 2.4, using the sole modal signal to close a static feedback control loop at the system input ($\#d$) may be modeled as

$$u_d = P_d \sum_q K_{d,q} \boldsymbol{C}_q \boldsymbol{m}_j z_j \tag{2.8a}$$

$$O_d = P_d \sum_q K_{d,q} \boldsymbol{C}_q \boldsymbol{m}_j \tag{2.8b}$$

where u_d is a synthesized modal signal of mode j scaled by a gain P_d, $K_{d,q}$ denotes the gain for the modal signal in system output y_q, and O_d represents the scaled modal observability. The controller is depicted in Fig. 2.1.

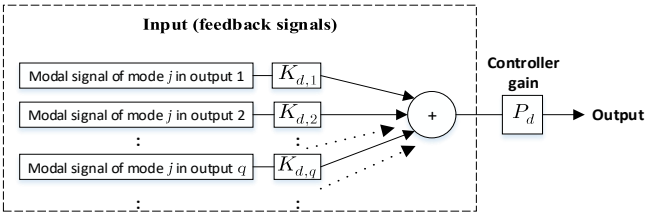

Figure 2.1: The controller for the j^{th} mode at system input ($\#d$).

For the sake of illustration, consider that the j^{th} mode is controlled by two controllers, i.e., the controllers at u_1 and u_2 access the modal signal of the j^{th} mode, the closed-loop system state matrix in the new coordinates is

$$\boldsymbol{A}^* = \begin{bmatrix} \lambda_1 & 0 & \cdots & \boldsymbol{n}_1^T \boldsymbol{B}_1 O_1 + \boldsymbol{n}_1^T \boldsymbol{B}_2 O_2 & \cdots & 0 \\ 0 & \lambda_2 & \cdots & \boldsymbol{n}_2^T \boldsymbol{B}_1 O_1 + \boldsymbol{n}_2^T \boldsymbol{B}_2 O_2 & \cdots & 0 \\ \vdots & \vdots & \ddots & \vdots & \ddots & \vdots \\ 0 & 0 & \cdots & \lambda_j + \boldsymbol{n}_j^T \boldsymbol{B}_1 O_1 + \boldsymbol{n}_j^T \boldsymbol{B}_2 O_2 & \cdots & 0 \\ \vdots & \vdots & \cdots & \vdots & \ddots & 0 \\ 0 & 0 & \cdots & \boldsymbol{n}_n^T \boldsymbol{B}_1 O_1 + \boldsymbol{n}_n^T \boldsymbol{B}_2 O_2 & \cdots & \lambda_n \end{bmatrix} \tag{2.9}$$

It can be seen from (2.9) that the controllers will only alter the j^{th} mode and the modified mode is given by $\lambda_j + \boldsymbol{n}_j^T \boldsymbol{B}_1 O_1 + \boldsymbol{n}_j^T \boldsymbol{B}_2 O_2$, which implies that the damping control actions are fully decoupled and therefore: each controller is allowed to independently set up

its contribution to the mode by adjusting the gain P; adding or missing any controller will not affect the effort of the other controllers.

The above control strategy may be extended to the control of multiple modes. Again, for ease of illustration, consider that two modes, e.g., modes #1 and #2, are controlled by four controllers, respectively. In particular, the controllers at u_1 and u_2 access the modal signal of mode #1, the controllers at u_3 and u_4 access the modal signal of mode #2. The modified modes can be obtained by solving the eigenvalues of a subset of the closed-loop system state matrix, denoted as

$$\boldsymbol{A}_s^* = \begin{bmatrix} \lambda_1 + a_{11} & a_{12} \\ a_{21} & \lambda_2 + a_{22} \end{bmatrix} \tag{2.10}$$

where

$$\begin{aligned} a_{11} &= \boldsymbol{n}_1^T \boldsymbol{B}_1 O_1 + \boldsymbol{n}_1^T \boldsymbol{B}_2 O_2; \\ a_{12} &= \boldsymbol{n}_1^T \boldsymbol{B}_3 O_3 + \boldsymbol{n}_1^T \boldsymbol{B}_4 O_4; \\ a_{21} &= \boldsymbol{n}_2^T \boldsymbol{B}_1 O_1 + \boldsymbol{n}_2^T \boldsymbol{B}_2 O_2; \\ a_{22} &= \boldsymbol{n}_2^T \boldsymbol{B}_3 O_3 + \boldsymbol{n}_2^T \boldsymbol{B}_4 O_4. \end{aligned}$$

Ideally, if the off-diagonal terms of (2.10) are inherent zeros, the controllers for the same mode and different modes are fully decoupled, because the eigenvalues of $\boldsymbol{A}_s^*$ are given by its diagonal terms. But, in reality, the off-diagonal terms may be non-trivial complex numbers. Moreover, it is noted that the Os in (2.10) are non-trivial numbers as they are designed to modify the modes. So, to apply the proposed strategy to control both modes, $\boldsymbol{A}_s^*$ should be at least nearly either a lower or upper triangular matrix; then, the eigenvalues of $\boldsymbol{A}_s^*$ can be approximately given by its diagonal terms. To this end, the controllers that target mode #2 may need to be enabled at places that have small controllability for mode #1; then the cross modal terms induced by the control of mode #1 is no longer crucial in terms of modal interactions. Moreover, if the natural frequency of mode #1 is close to the frequency of mode #2, then both a_{12} and a_{21} may need to be small, which requires that the control sites for mode #1 also have small controllability for mode #2.

2.6 APPLICATION TO MULTI-POINT ACTIVE POWER MODULATION

Active power modulation may be executed by a system device that has fast power response capability, e.g., energy storage system. The dynamics of the power modulation may be modeled as a first order transfer function [38], as depicted in Fig. 2.2. When a controller in Fig. 2.1 is connected to P_{ref}, as the system is excited, the device will provide a stabilizing signal $\Delta P_{in}(t)$ to the system. This type of modulating control is physically interpretable, it has been well observed from the experiments that a qualified control signal tends to be out of phase with the oscillation signal seen by the device's terminal bus frequency, which indicates that the device will dissipate the oscillation energy or say provide damping torque to the oscillation.

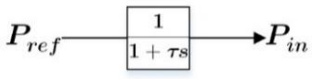

Figure 2.2: Simplified active power modulation block.

When applying the proposed strategy to control a group of such devices to damp a particular mode of frequency oscillation (electromechanical or common low-frequency), the power modulations may be engineered by employing the following method.

For a particular mode of oscillation, because the outputs of the controllers are in proportion to their respective O_d, to pursue consistent amplitude of power response $|\Delta P_{in}|$ for all the devices, the gains of the controllers may be set up according to

$$\frac{\left|\boldsymbol{n}_j^T \boldsymbol{B}_1 O_1\right|}{\left|\boldsymbol{n}_j^T \boldsymbol{B}_2 O_2\right|} = \frac{\left|\boldsymbol{n}_j^T \boldsymbol{B}_1\right|}{\left|\boldsymbol{n}_j^T \boldsymbol{B}_2\right|} \tag{2.11}$$

Equation (2.11), which is equivalent to $|O_1|=|O_2|$, ensures that the damping contributions are allocated according to the modal controllability. Furthermore, to impose constraints on the response of each device, choose

$$\frac{\left|\boldsymbol{n}_j^T \boldsymbol{B}_1 O_1\right|}{\left|\boldsymbol{n}_j^T \boldsymbol{B}_2 O_2\right|} = \frac{\varepsilon_1 \left|\boldsymbol{n}_j^T \boldsymbol{B}_1\right|}{\varepsilon_2 \left|\boldsymbol{n}_j^T \boldsymbol{B}_2\right|} \tag{2.12}$$

where ε may be the response limit of the device, denoted by $P_{max} - P_{ref}$. Clearly, $\varepsilon\left|\boldsymbol{n}_j^T \boldsymbol{B}\right|$ may serve as an index for selection of the actuators.

The actual power responses of the devices are determined by the closed-loop system dynamics. Larger gains of the controllers tend to result in larger power responses of the devices. However, it also means larger damping will be added to the target mode, which renders a mitigation effect on the maximum values and duration of the power responses. Moreover, the concerned mode of oscillation is usually triggered by a transient event occurs in the system. In this regard, stimulation of the system at different locations in a non-linear simulation environment may be necessary to properly set up the gains of the controllers. The main tuning involved will be adjusting the weights in (2.12) and simultaneously scaling the gains of the controllers. Note that the damping that the controllers can provide is mainly dependent on the availability of the supporting devices and how large the oscillation will be under the most severe contingency. As more devices partake in the control of a mode, the damping contribution needed from each device can be smaller, therefore smaller pressure put on the individual devices. Automation of the gain tuning process may deserve further study.

For a large power system with geographically dispersed actuators, the multi-mode control strategy may be applied. This is based on the fact that the electromechanical modes are usually controllable at some particular sites (areas) and the common low-frequency mode is widely controllable at the system interconnection buses. So, it is possible to group the devices to simultaneously control multiple modes with less control interactions. However, as set forth in the previous section, the decoupled multi-mode control requires a stricter actuator selection that may sacrifice the optimality of the control of each single mode in terms of the asset utilization. Nevertheless, under certain circumstances, e.g., when pursuing simultaneous control of electromechanical oscillations and the transient frequency swing and/or control of closely spaced inter-area modes of oscillations with explicit control cost allocation and robustness to disturbances, the proposed strategy may be an option. Optimization of the multi-mode control strategy may deserve further investigation.

2.7 DETERMINATION OF THE INPUT SIGNALS USING LQRSP

In (2.9), the proposed damping controller needs to access a pure modal signal to achieve the respective mode mobility. But, it may be difficult to realize this in practice. Therefore, the goal here is to help the controllers access a modal selective signal whose modal observability is dominated by the target mode. In static feedback control, this may be accomplished by carefully pairing the system outputs and inputs. For instance, using $\sum_q K_{d,q}\boldsymbol{C}_q\boldsymbol{x}$ to obtain an input signal, which features $\left|\sum_q K_{d,q}\boldsymbol{C}_q\boldsymbol{m}_j\right| \gg \left|\sum_q K_{d,q}\boldsymbol{C}_q\boldsymbol{m}_r\right|$ for any mode r, for the purpose of improving the damping of the j^{th} mode. Nevertheless, it is not easy to achieve this for a large power system without the help of a systematic algorithm, as each system state may significantly participate in multiple mode dynamics, which can be seen from (2.2). Ideally, we expect a solution so that the required system outputs are readily accessible via the ever maturing dynamic state estimators [43], e.g., the rotor speed. As follows, the LQRSP technique [44] is formalized as a tool for determining the desired input signal using the least number of system states.

a) Brief Review of the LQRSP: If we consider that the system output in (2.1b) is a combination of full system states, i.e., the state vector is observed by an $n \times n$ identity matrix, the LQR-based sparsity-promoting optimal control problem can be formulated as [45]:

$$\begin{cases} \text{minimize } \lim\limits_{t\to\infty} \varepsilon\{\boldsymbol{x}(t)^T\boldsymbol{Q}\boldsymbol{x}(t) + u(t)^T\boldsymbol{R}u(t)\} \\ \qquad\qquad +\gamma\sum\limits_{i,j} w_{i,j}\left|F_{i,j}\right| \\ \qquad\qquad \text{subject to} \\ \text{dynamics: } \dot{\boldsymbol{x}}(t) = \boldsymbol{A}\boldsymbol{x}(t) + \boldsymbol{B}_{s1}u(t) + \boldsymbol{B}_{s2}\eta(t) \\ \qquad\qquad \text{linear control: } u(t) = -\boldsymbol{F}\boldsymbol{x}(t) \\ \text{stability: the real parts of } eig(\boldsymbol{A} - \boldsymbol{B}_{s1}\boldsymbol{F}) < 0 \end{cases} \tag{2.13}$$

where $\varepsilon\{\cdot\}$ is the expectation operator, $\boldsymbol{Q}$ is an $n \times n$ positive semi-definite matrix designed to penalize particular system dynamics, $\boldsymbol{R}$ is a $p \times p$ positive definite matrix, and p is the number of system inputs selected to equip controllers, for our distributed controller design, $p = 1$. Normally, the matrix $\boldsymbol{R}$ is an identity matrix, and $\boldsymbol{B}_{s1} = \boldsymbol{B}_{s2}$ with $\boldsymbol{B}_{s1}$ as the control input vector and $\boldsymbol{B}_{s2}$ as the disturbance input vector. $\gamma\sum_{i,j} w_{i,j}\left|F_{i,j}\right|$ is the sparsity promoting function, $w_{i,j}$ is the weight on the corresponding gains $F_{i,j}$, and γ is usually a small positive number within a range to promote the sparsity of the gain matrix $\boldsymbol{F}$. For $\gamma = 0$, the control

reduces to a standard H_2 optimal control problem, the optimal gain matrix $\boldsymbol{F}_c$ can be obtained by solving the Algebraic Riccati Equation (ARE), and $\boldsymbol{F}_c$ is usually fully populated with non-zero entries. By gradually increasing γ, the sparsity promoting process tends to strike a balance between the dynamic response performance and the number of communication links (i.e., the number of non-zero entries of $\boldsymbol{F}$). The algorithm is available in Matlab as *lqrsp*.

b) LQRSP as a Tool for Determining the Modal Selective Signal: In [45], the authors mentioned that the sparse LQR may be modal selective by using a proper state cost function, e.g., the state cost can be squared relative rotor speed and angle between two groups of machines for the purpose of controlling a specific inter-area mode. Thus inspired, two types of state costs are employed below to search the desired input signals for the controllers.

For the control of an electromechanical mode, choose

$$\boldsymbol{x}^T\boldsymbol{Q}\boldsymbol{x} = \zeta\left(\omega_\alpha - \omega_\beta\right)^2 \tag{2.14}$$

And for the control of the common low-frequency mode, choose

$$\boldsymbol{x}^T\boldsymbol{Q}\boldsymbol{x} = \zeta(\omega_{\mathrm{COI}})^2;\ \omega_{\mathrm{COI}} = \frac{\sum_{\alpha=1}^{n_m} H_\alpha\omega_\alpha}{\sum_{\alpha=1}^{n_m} H_\alpha}. \tag{2.15}$$

where ω_α and ω_β denote a pair of (aggregated) synchronous machine speed variables that oscillate against each other under a particular inter-machine oscillation, n_m is the amount of synchronous machine in the system, and ζ is a scalar; ω_{COI} denotes the center-of-inertia (COI) speed of the system, H_α and ω_α denote respectively the inertia time constant and the speed variable of synchronous machine α.

c) Interpretation: Given that the LQR can be viewed as a controller that intends to shrink the energy of the input-output frequency response [46], the following inference may serve as an interpretation of the approach. Based on (2.3a), (2.3b) and the modal properties, and assuming zero initial conditions, a unit impulse in the selected input yields the following responses in the i^{th} output

$$y_i(t) = \sum_{j=1}^{n} \boldsymbol{C}_i\boldsymbol{m}_j\boldsymbol{n}_j^T\boldsymbol{B}_{s1}e^{\lambda_j t} \tag{2.16}$$

Therefore, a particular mode may dominate a synthesized output response by linearly combining the responses of different system outputs. Using (2.14), the response of the common mode tends to be excluded while the response of a particular inter-machine mode is emphasized. Using (2.15), the responses of inter-machine modes are greatly eliminated while the response of the common mode is retained as the speed variables oscillate coherently under the common mode dynamics. According to (2.6) and (2.7) and following the logic of the LQR control, it can be inferred that if the impulse response of a system output is dominated by a single mode, then the controller tends to find a gain matrix that stresses the modal signal of the dominant mode while excluding the other modal signals. Because excessive modal signals of non-dominant modes will increase the control energy yet are unable to reduce the response energy of the dominant mode, and hence the overall energy, the result is the desired input signal.

d) Practical Considerations: In practice, a proper transient stability model should be prepared and updated; this is beyond the scope of this chapter but has been routinely utilized in power system operations and planning. Standard linearization techniques may be employed to obtain the state-space model. When carrying out the LQRSP, the modal selectivity of the input signal tends to be perfect by using the optimal gain matrix; the interaction among the controllers, which violates the decoupling goal, tends to increase as the modal selectivity deteriorates. Therefore, a trade-off occurs between the desired control performance and the sparsity of the gain matrix for each controller. As confirmed later, the presented approach helps to find the desired input signal for a controller resulting from a linear combination of the states of the systems. And, thanks to the sparsity-promoting technique, all the controllers need to access rotor speed variables of the synchronous generators but without sacrificing the optimal control performance possibly because of the modal structure of the modes. Despite wide-area signals being required, the LQR-based implementation, which guarantees phase margin, ensures that the control system is robust to the communication delays as demonstrated in [45]. In addition, the selection of α and β in (2.14) is the result of modal structure investigation and coherency grouping, prior know-ledge of the system is preferred; a linear combination of frequency differences that mimics the relative speed of the oscillating areas is suggested for setting up the state cost, as the common mode is usually the main contributor to the input-output dynamics. The use of

LQRSP to simultaneously determine the input signals for a set of controllers by combining the control inputs into a single LQR may also be feasible, however, the distributed formulation presented represents an opportunity for parallel implementation of the input signal determination for a large set of controllers. A systematic algorithm is desired to automate the input signal determination process.

2.8 DAMPING CONTROLLER DESIGN FLOWCHART

A design procedure for the damping controllers for a particular mode is summarized in Fig. 2.3. Steps 1-2 aim to prepare the linear model and choose control locations for the concerned mode. Steps 3-4 are related to the determination of the input signal for each controller; as usual in control design trial and error might be encountered especially for the parameters used in the LQRSP algorithm. Steps 5-6 are devoted to the gain tuning.

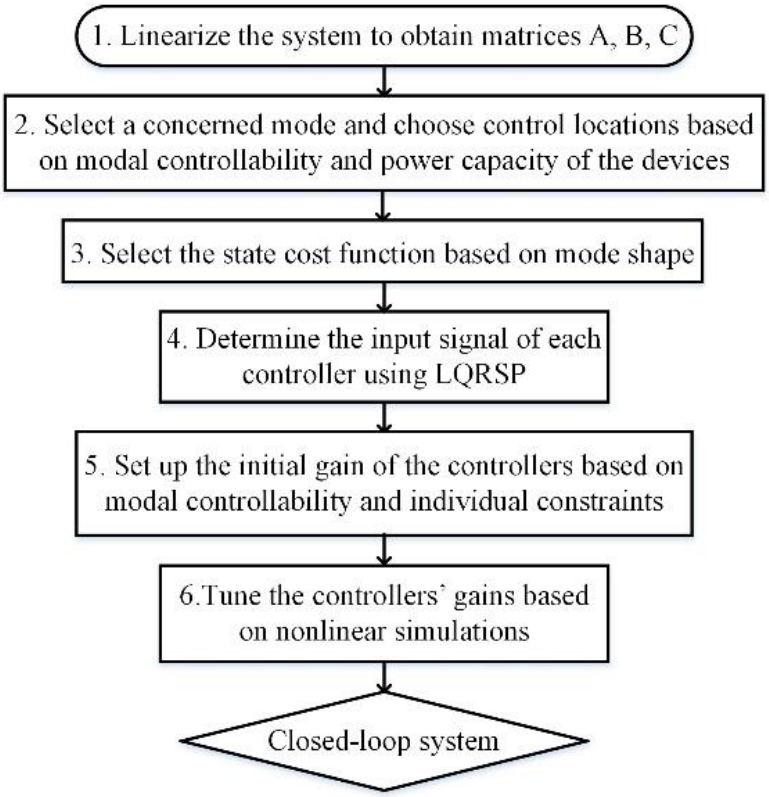

Figure 2.3: Design flowchart of the damping controllers for a particular mode.

2.9 SYSTEM DESCRIPTION

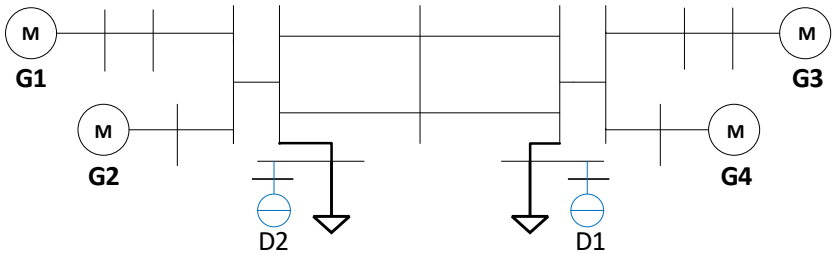

Figure 2.4: Two-area system. D1 and D2 are the integrated power devices.

Table 2.1: Electromechanical Modes and the Common Mode

Modes	Eigenvalues
Local 1 (G1 vs G2)	–0.5344 + 7.2711i
Local 2 (G3 vs G4)	–0.8146 + 8.0112i
Inter-area (G1,G2 vs G3,G4)	**–0.0414 + 4.1733i**
Common (Coherent)	–0.4720 + 0.3909i

Kundur's two-area system in [23] is adapted for a detailed validation of the proposed methodology with the help of Power System Toolbox [22]. Two active power injection devices are integrated into the system near the loads as depicted in Fig. 2.4. The devices are both operating at 20 MW. For illustration purposes, there is no response limit assigned to the devices. The generators are modeled using a sub-transient generator model (6^{th} order). Simple exciter (1^{st} order) is installed on the generators. Simple turbine-governor model (3^{rd} order) is employed to model the mechanical power dynamics of the generators. No PSS is enabled. The loads are modeled as constant impedance loads for both the active and reactive power consumptions. Eigen-analysis reveals that the system is stable, and the electromechanical modes and the common mode are listed in Table 2.1. It is seen that the system's inter-area mode is lightly damped due to possibly the heavy power transfer and the fast-acting voltage regulators. The goal here is to damp the inter-area oscillation by efficiently modulating the active power injections of the integrated devices.

2.10 EMPIRICAL STRATEGIES

Before proceeding, to gain some insights into the necessity of a scientific control design, some empirical output feedback strategies are reviewed. For a static feedback control loop that is established between the specified system output and the power set point of D2, the root-locus is depicted in Fig. 2.5. Although all of the strategies can improve the damping of the inter-area mode, several important issues are noteworthy:

1) When using the rotor speed of generator 2 as control input, the inter-area mode obtains relatively small mode mobility compared to the common mode and local mode 1. So, to achieve a desired damping improvement of the inter-area mode, excessive control energy may be consumed by those two well-damped modes.
2) The 'local average speed' $\omega_1 + \omega_2$ removes the local mode mobility, but the common mode mobility is still relatively large.
3) The 'local speed difference' $\omega_1 - \omega_2$ destabilizes the local mode while adding small damping to the inter-area mode. In addition, $\omega_2 - \omega_1$ stabilizes local mode 1 while destabilizing the inter-area mode.
4) The 'speed difference' $\omega_1 - \omega_3$ slightly degrades the damping of local mode 1. Therefore, the damping improvement of the inter-area mode needs to be limited in order to alleviate the side-effect on the local mode.

The similar results are observed for D1. Moreover, the movement of system modes on the complex plane may be more complicated when multiple devices partaking in the control of a more complex system. In the following, the proposed method is first applied, and then it is compared with the optimal control strategy in [45], which suggests a feedback that controls both the inter-area mode and the common mode. The usefulness of the proposed method can be illustrated from this comparison.

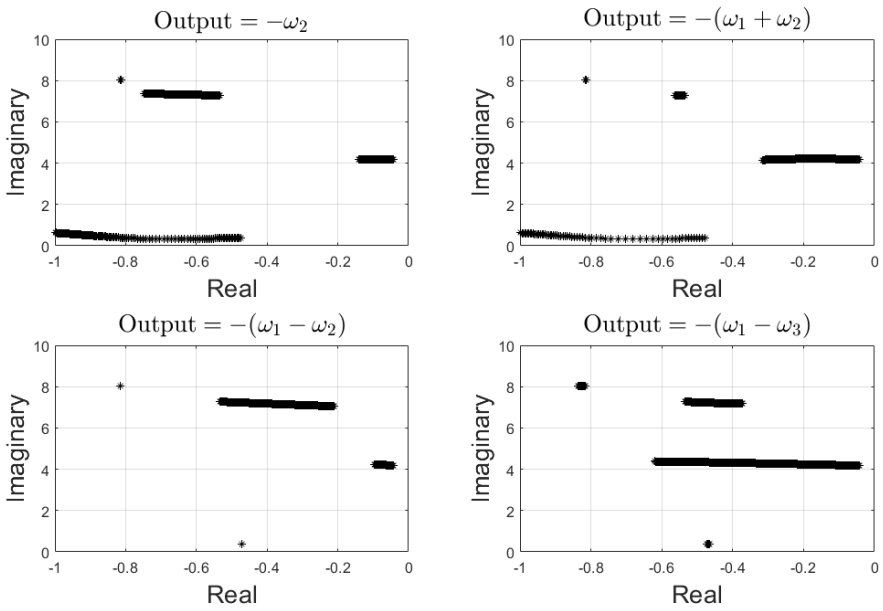

Figure 2.5: Root locus, two-area system case.

2.11 PROPOSED SOLUTION

For illustration purposes, the design process of controller 1 (C1) for D1 is detailed here. $\zeta(\omega_1 - \omega_3)^2$ is chosen as the state cost for the LQR, where ω_1 and ω_3 denote respectively the rotor speed variables of generators 1 and 3. The magnitude frequency response of the open-loop transfer between the device's power set point and the synthesized output $\omega_1 - \omega_3$ is shown in Fig. 2.6. The inter-area mode dominates the response, so it is expected that the resulting gain matrix of the LQR with 40 logarithmically spaced values, the LQRSP delivers following information. As shown in Fig. 2.7, for $\gamma = 0$, the gain matrix given by ARE is fully populated and, as γ increases, the number of non-zero entries of the gain matrix is greatly reduced while the control performance slightly deteriorates. For $\gamma = 0.1$, the gain vector is $\boldsymbol{F}_{\gamma=0.1} =$ [0.0002, –1.1139, **0**, –1.0413, **0**, 1.1873, **0**, 1.0431, **0**], where **0** denotes zeros, the four relatively large numbers are the gains for the rotor speed variables of generators 1-4, respectively. The relatively small number is the gain for the rotor angle state of generator 1. It is very small, thus it is reasonable to remove it from the gain vector. Therefore, the gain vector selected for C1 is $\boldsymbol{F}_s =$[0, –1.1139, **0**, –1.0413, **0**, 1.1873, **0**, 1.0431, **0**], which means that the input signal of the controller in Fig. 2.1 is $1.1139\omega_1(t)$+$1.0413\omega_2(t)$–$1.1873\omega_3(t)$–$1.0431\omega_4(t)$.

The ideal closed-loop system modes given by $eig(\boldsymbol{A} - 58\boldsymbol{B}_{D1}\boldsymbol{F}_s)$ are depicted in Fig. 2.8; #58 is the controller gain. It can be seen that only the inter-area mode is significantly modified indicating the modal selectivity of the input signal. To verify the theoretical derivation, the mode-move calculated by the scaled mode mobility in (2.9) is given in (2.17).

$$\begin{aligned}(\boldsymbol{n}_{inter}{}^{T}\boldsymbol{B}_{D1}) \times 58(1.1139\boldsymbol{C}_{spd1}\boldsymbol{m}_{inter} + \\ 1.0413\boldsymbol{C}_{spd2}\boldsymbol{m}_{inter} - 1.1873\boldsymbol{C}_{spd3}\boldsymbol{m}_{inter} - \\ 1.0431\boldsymbol{C}_{spd4}\boldsymbol{m}_{inter}) = -0.1973 + j0.0531\end{aligned} \tag{2.17}$$

The controller 2 (C2) for D2 is designed by following the same procedure, and the gain of the controller is tuned based on (2.11) using C1 as a reference. So, the devices are expected to have a similar amplitude of power response during the modulation process. The modes of the closed-loop system with C2 and that with two controllers are also depicted in Fig. 2.8, respectively.

Non-linear simulations are carried out to show the impact of the controllers on the system's oscillatory dynamics. At 2 s, the system is excited by a step increase in the exciter reference of generator 2. Under such type of disturbance, the system will undergo a process of converging to a new synchronous reference. This, however, alters the linear time invariant system assumption that the control approach relies on. Nevertheless, such disturbance provides an opportunity to examine the performance of the controllers when the synchronous reference varies within a small range, which is the nature of a real power system. In this chapter, the rotor speed variables are captured by differentiating each rotor speed from a common reference (i.e., 1 p.u.). The relative speed of generators 1 and 3 is plotted in Fig. 2.9. It evidently shows that the controllers work in a superposition manner to damp the inter-area oscillation. The COI speed in Fig. 2.10 shows that the controllers have almost no influence on the trajectory of the system's synchronous reference. Indeed, as shown in Fig. 2.8, the controllers have trivial influence on the system's common mode, which defines the shape of a small-signal frequency swing [47] (chapter 1). Fig. 2.11 shows the devices' power responses during the modulation process, which indicates that only the oscillation signal of the inter-area mode is passing through the controllers and the gain tuning for shaping the power responses is effective. The disturbance significantly excites local mode 1 and the oscillation dictates the initial evolution of the relative speed of generators 1 and 2, as shown

in Fig. 2.12, which indicates that the modulations have a trivial effect on the mode dynamics. It is commonly recommended that synchronous machines take responsibility for mitigating the local mode of oscillations via modulation of their excitation systems, if necessary.

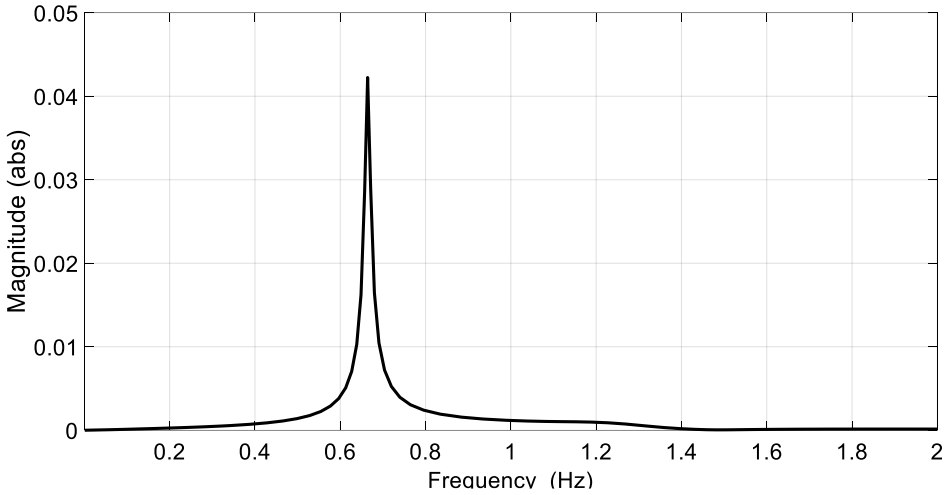

Figure 2.6: Magnitude frequency response of the open-loop transfer.

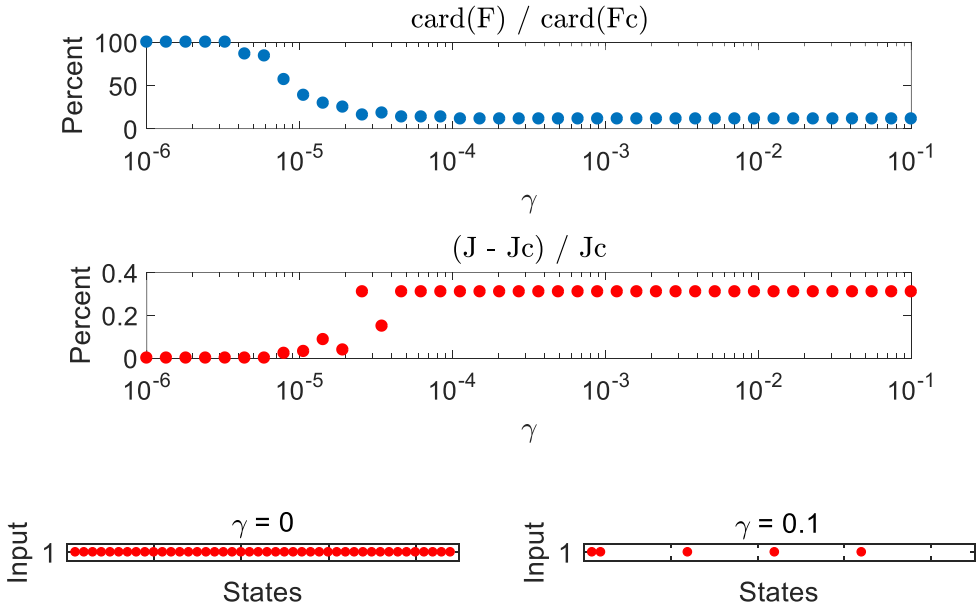

Figure 2.7: Sparsity-promoting results. card = cardinality. $(J - J_c)/J_c$ denotes the quadratic performance degradation of a sparse gain matrix $\boldsymbol{F}_s$ relative to the optimal gain matrix $\boldsymbol{F}_c$.

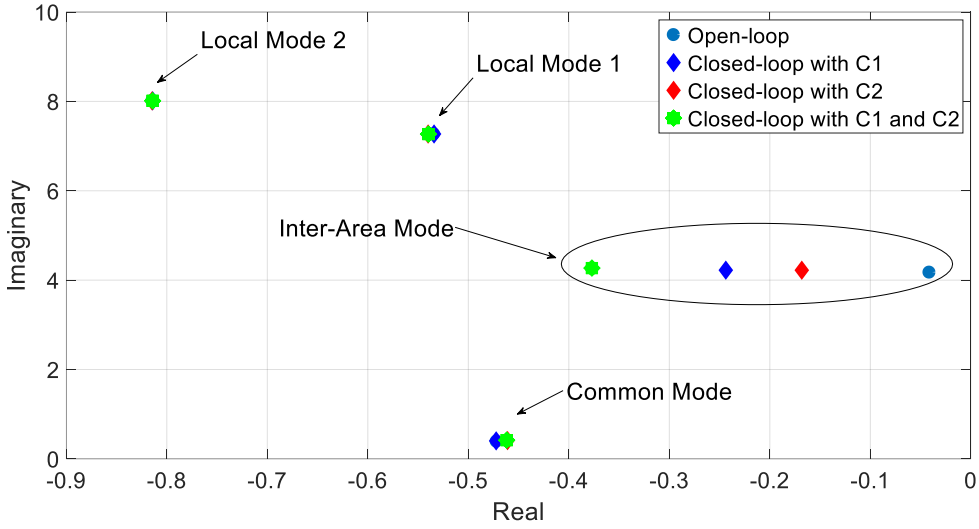

Figure 2.8: Closed-loop system modes.

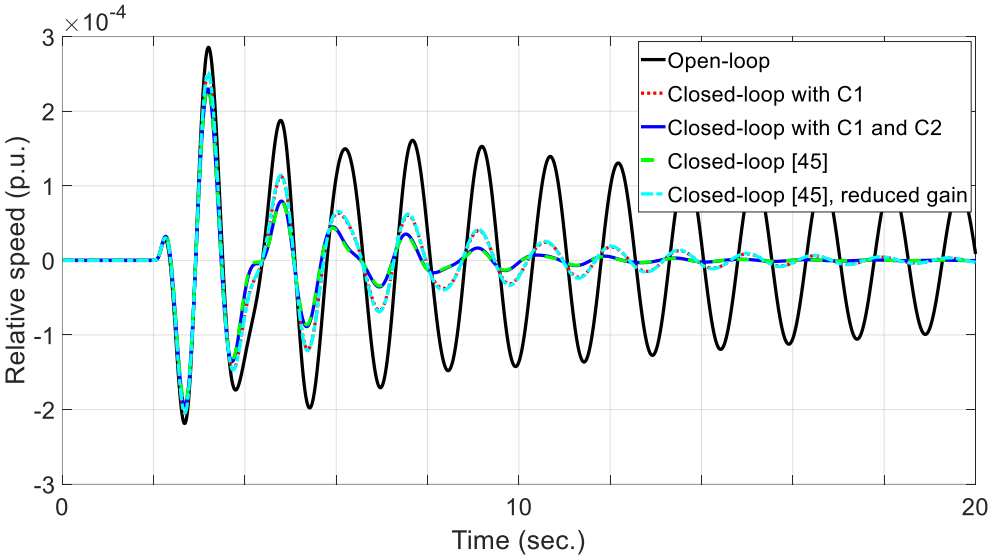

Figure 2.9: Relative speed of generators 1 and 3.

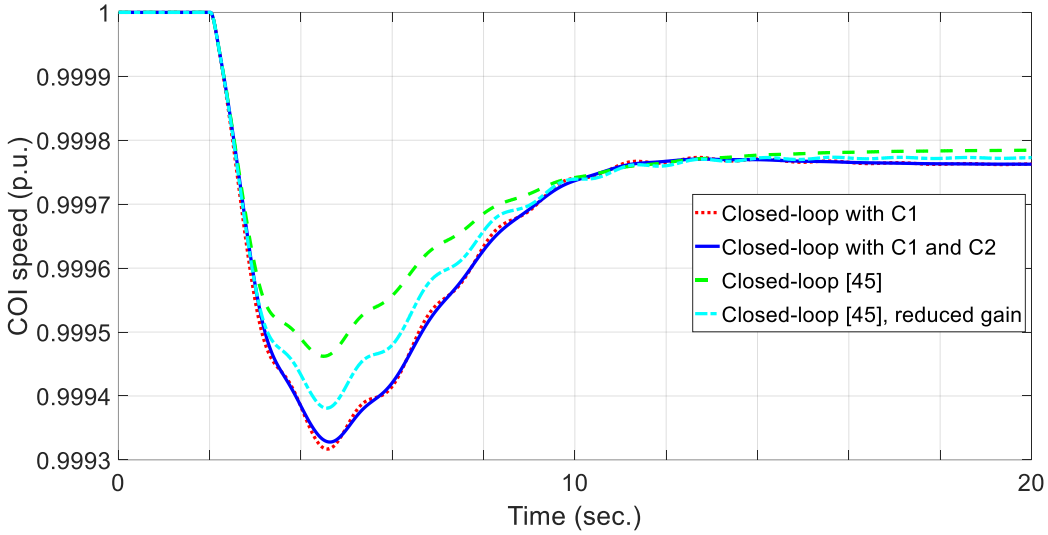

Figure 2.10: COI speed.

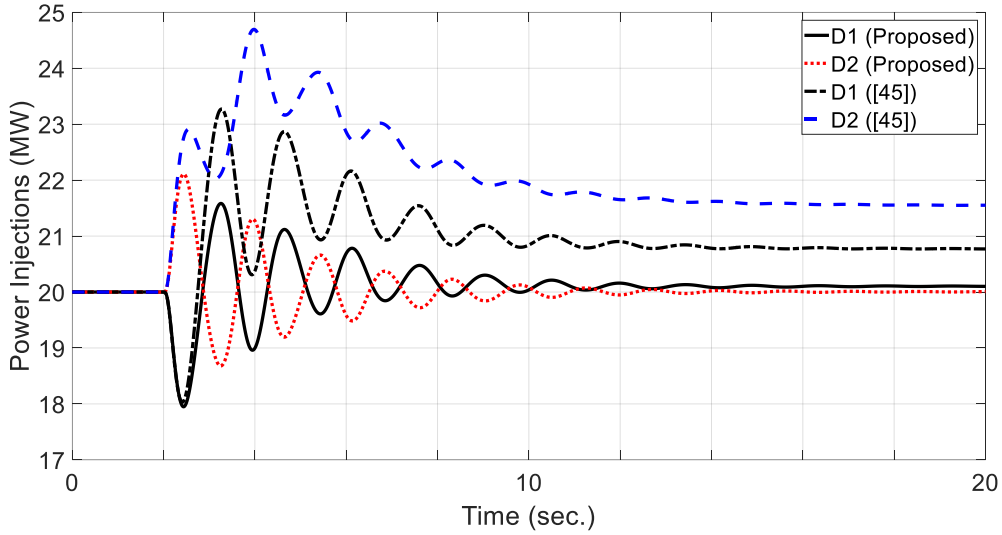

Figure 2.11: Power responses of the devices. Proposed method vs [45].

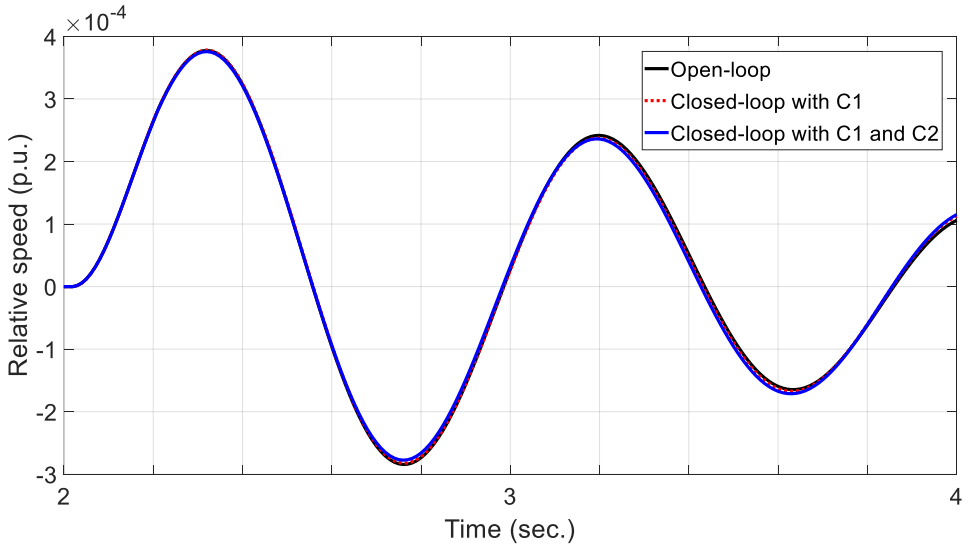

Figure 2.12: Relative speed of generators 1 and 2.

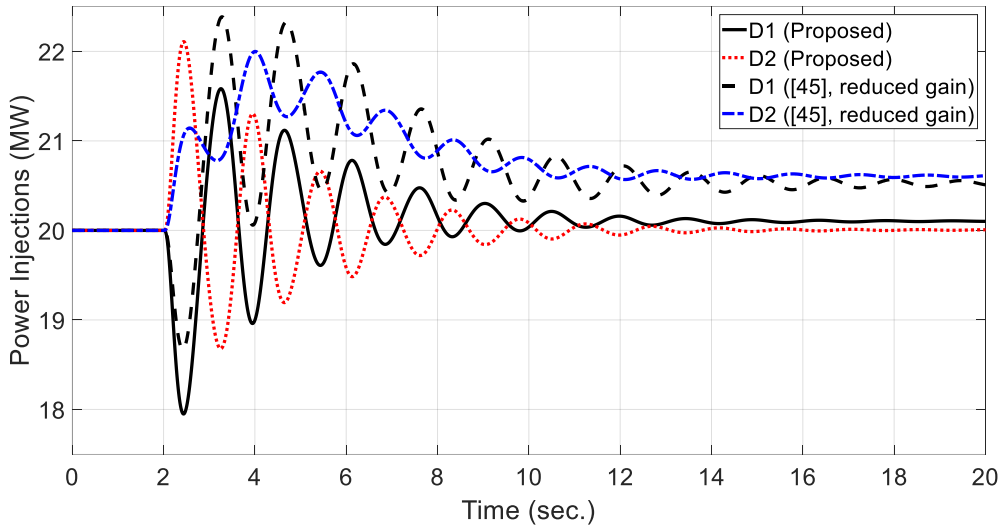

Figure 2.13: Power responses of the devices. Proposed method vs [45] with reduced gain.

2.12 COMPARISON WITH AN EXISTING OPTIMAL CONTROL STRATEGY

The power devices are enabled for implementing a sparse LQR with the optimal control strategy in [45], i.e., the $\boldsymbol{R}$ in (13) is now a 2×2 identity matrix; and the state cost is $\boldsymbol{x}^T \boldsymbol{Q} \boldsymbol{x} = \zeta(\sum_{\alpha=1}^{4} {\omega_\alpha}^2)$. Sparsity-promoting results show that the controller tends to access the four generator speed variables (the same communication cost as that required by the proposed controllers) without sacrificing the optimal control performance. The resulting controller is tested by the same disturbance. As shown in Figs. 2.9-2.11, the controller takes more control energy from the devices to achieve the same damping improvement for the inter-area mode as done by the proposed controllers. This is because some control energy are spent on controlling the common mode; however, the improvement of the system's primary frequency response is not very significant besides the frequency nadir. Moreover, if the devices are not ready to permanently increase/decrease their power injections (e.g., due to economic dispatch), the control actions will be infeasible. In the standard (sparse) LQR design, the (near) optimal gain array is fixed for a given performance index, and there is no standard guideline for accommodating the input constraints; however, this case study shows the controller gains have some flexibility with respect to tuning without altering the control effect (controlling the common mode and the inter-area mode), possibly due to the simple control structure, modulation type and location, and the distinct frequencies of the two modes. The inter-area mode was therefore moved so that its damping is close to that obtained by the proposed controllers. Given that in static feedback control the eigenvectors of the system state matrix are fixed, the traces in Fig. 2.9 for the 'Closed-loop with C1 and C2' and 'Closed-loop with [45]' cases nearly coincide with each other.

By reducing accordingly the gain for the power command signal for each device, as shown in Fig. 2.13, the maximum power responses are aligned with that commanded by the proposed controllers; however, there are still non-trivial steady-state bias, and the effect that the controller has on the inter-area mode is reduced, as shown by the relative generator speed in Fig. 2.9 and the tails of the power responses in Fig. 2.13.

2.13 SIMULATION ON A LARGE SYSTEM

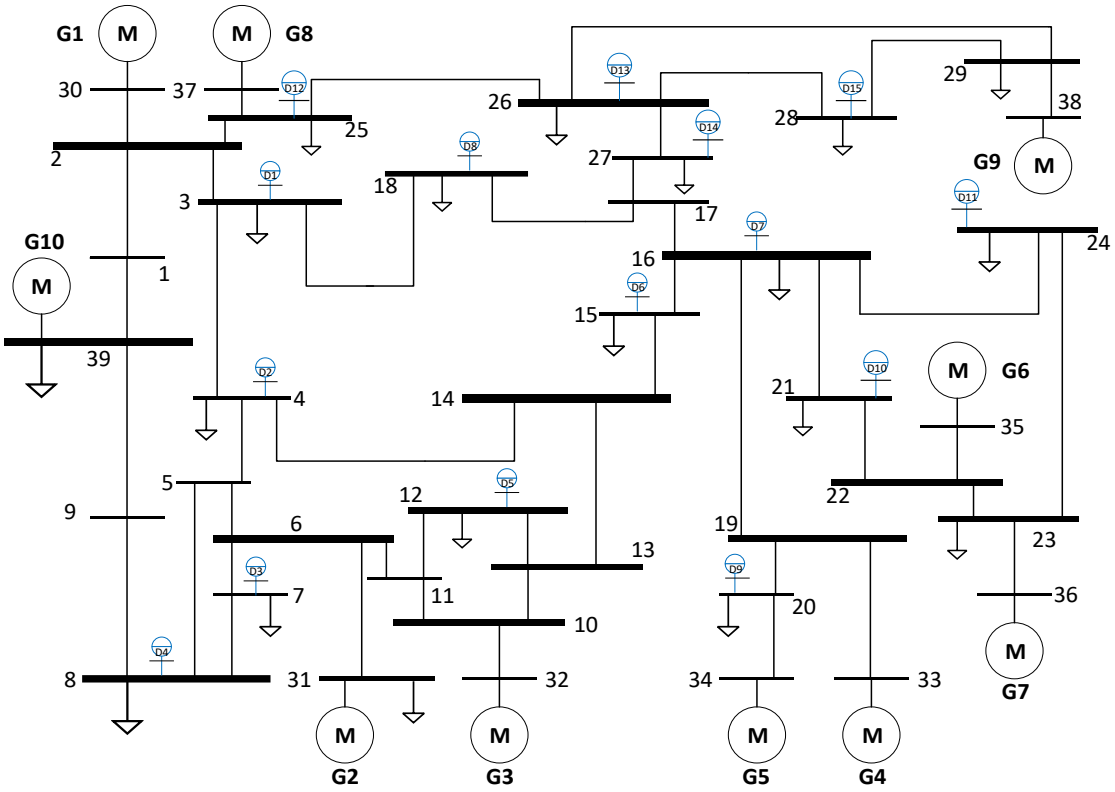

Figure 2.14: New England 39-bus system. Blue circles denote the integrated active power injection devices.

To examine the applicability and scalability of the control approach, a study on the New England 39-bus system is carried out. 15 active power injection devices are integrated into the system, as depicted in Fig. 2.14. For illustration purposes, there is no response limit assigned to the devices. The power export of the NE system, i.e., $P_{1-39} + P_{9-39}$, exhibits a large swing under a power imbalance event; careful examination reveals that the swing is mainly governed by the 0.6 Hz inter-area mode and the system's common mode. The goal here is to mitigate the swing of this key power transfer by commanding the power injections of the 15 devices with the proposed control strategy (a large swing may trigger the protection and therefore the cascading issues). According to the modal controllability shown in Fig. 2.15, devices {D1, D5–D15} are selected to improve the damping of the 0.6 Hz inter-area mode, the state cost is $\boldsymbol{x}^T\boldsymbol{Q}\boldsymbol{x} = \zeta\left(\frac{1}{9}\sum_{\alpha=1}^{9}\omega_\alpha - \omega_{10}\right)^2$; devices {D2–D4} are selected to

improve the damping of the common mode and equation (2.15) is employed as the state cost. Note that the selection is for illustration purposes and may not be the best one, as the two modes have distinct frequencies and other devices may be assigned to control the common mode without introducing significant modal interactions. However, care may need to be taken when the common mode dynamics become faster as the system inertia decreases. Again, optimization of the decoupled multi-mode control needs further investigation. After determining the input signals (only rotor speed variables are involved), the gains of the controllers are initially tuned based on (2.11) and then simultaneously scaled to achieve a desired damping for the respective mode. The 'root locus' depicted in Fig. 2.16 is obtained by simultaneously scaling the gains for two controllers of the two modes. The uniform motion of modes indicates that the modal controllers are nearly decoupled.

As shown in Figs. 2.17 and 2.18, in response to a sudden load increase in the NE part of the system, the devices gracefully modulate their power injections to damp their respective mode of oscillations. As a result, the swing of the power export of the NE system is reduced by about (peak-to-peak) 50 MW for this particular event and the tie-line power oscillations converge in 10 seconds. The power responses of {D2-D4} are large; however, the pressure of each device can be relieved if more devices nearby are responsive. It is worth emphasizing that the proposed decoupling control for electromechanical oscillations and the transient frequency swing only reduces the interactions from the viewpoint of a linear system and does not eliminate the interactions, as they are essentially non-linear dynamics, especially when the later one appears. In addition, a smoother frequency excursion may help the electromechanical controls behave properly, as the deviation of system frequency may drive the synchronous machines away from their operating points.

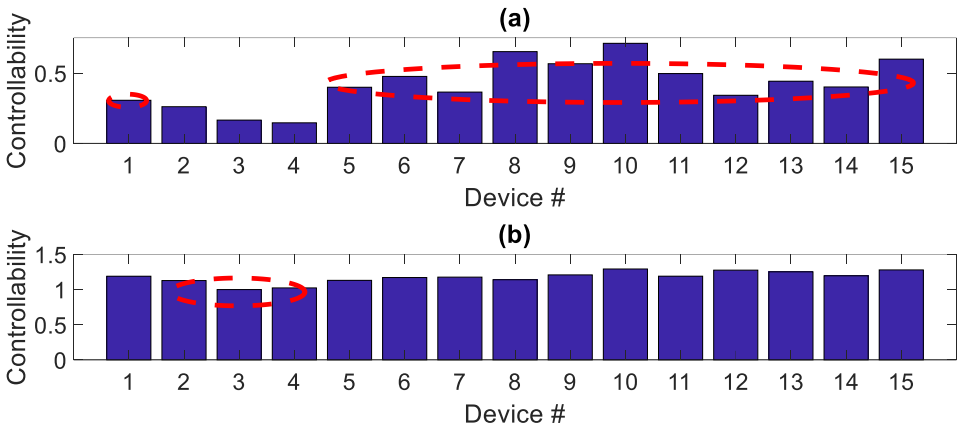

Figure 2.15: Modal controllability of the devices. (a) 0.6 Hz inter-area mode. (b) The common mode. Selected devices for controlling each mode are encircled.

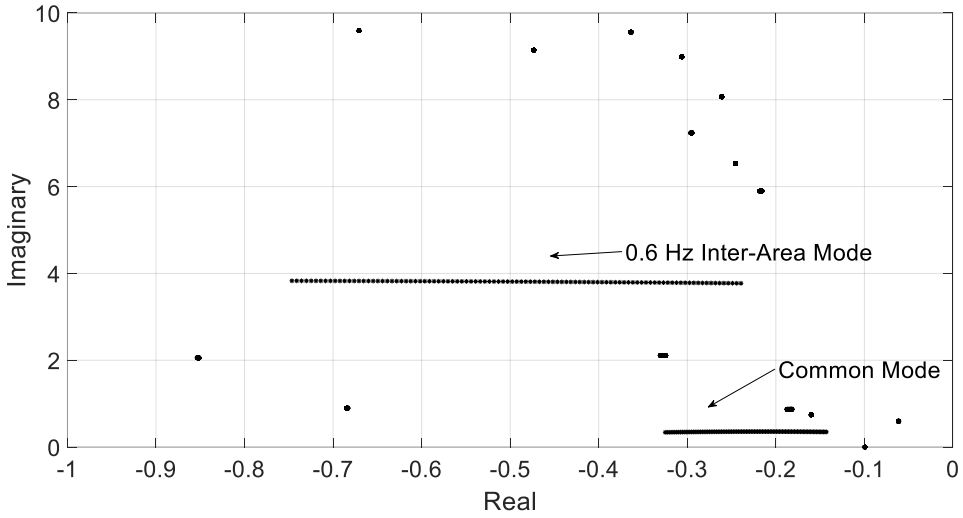

Figure 2.16: 'Root locus', New England 39-bus system case.

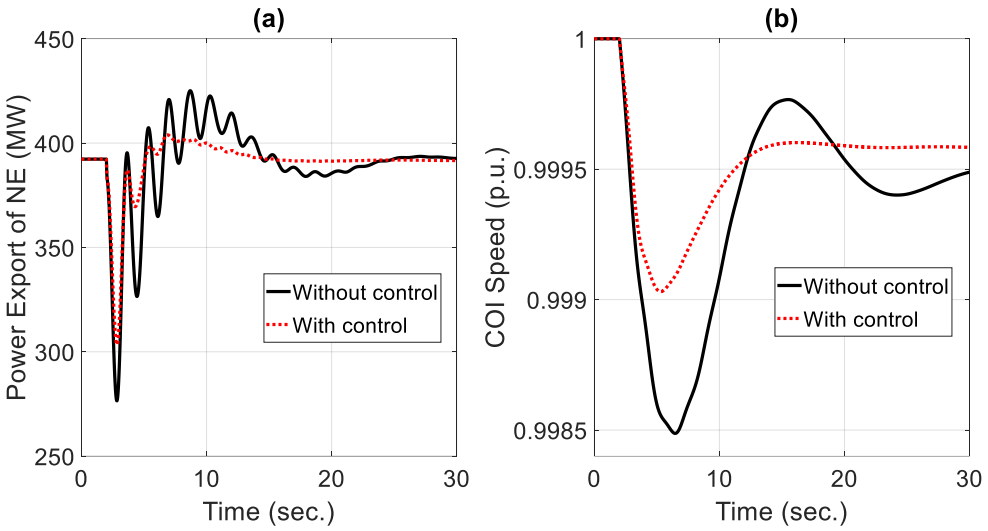

Figure 2.17: (a) Power export of the NE system. (b) COI speed.

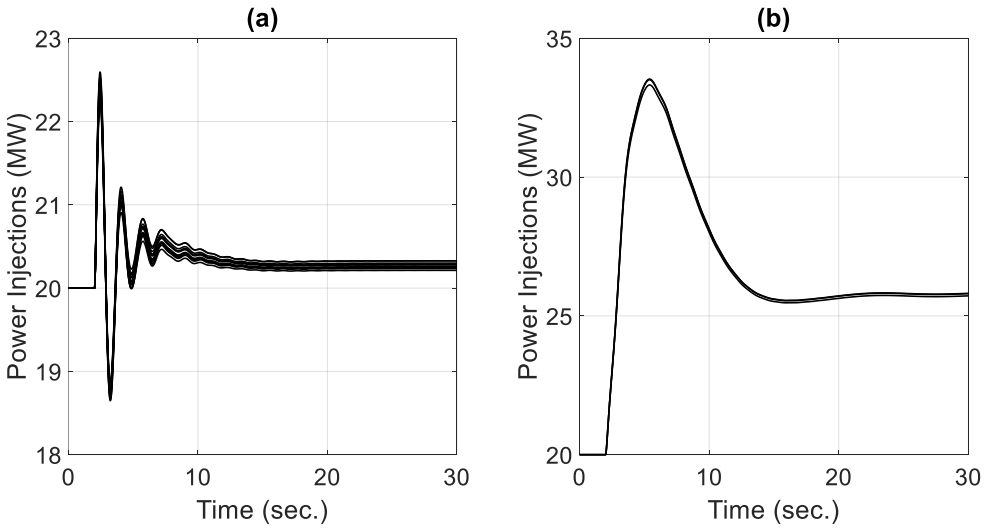

Figure 2.18: Power responses of the devices. (a) {D1, D5–D15}. (b) {D2–D4}.

2.14 SUMMARY

Based on the validation results, the advantages of the proposed control strategy may be briefly summarized as follows: It shows improved flexibility and efficiency than the conventional strategy in terms of mitigating the critical oscillation with bounded stabilizing signals. Because of the (verified) super-position feature, the single-point control energy can be greatly reduced if considerable devices partake in the control, thereby reducing the effects of control actions on the steady-state operation of the devices. These features may be favorable for the utilization of DERs in wide-area damping control, by which may help build a healthier power system damping structure.

The initial results showed that the approach has the potential to be a choice for system planners to unlocking large-scale DERs for damping control under particular operating conditions, with a unique advantage of distributing the control effort to many geographically dispersed sites so that small modulation is needed at each single site.

CONCLUSION

This dissertation provides a novel wide-area control strategy for damping of critical frequency oscillations via modulation of fast active power injections, which paves the way for the utilization of large-scale geographically dispersed actuators, e.g., distributed energy resources (DERs), in the control of power system low-frequency rotor angle dynamics, this includes the inter-area oscillations and the transient frequency swing. The proposed method incorporates the transient frequency swing into a linear time invariant (LTI) system based control framework, in which the control of the transient frequency swing is translated into the control of the system common mode dynamics. A careful examination of the relationship between the transient frequency swing and the common mode dynamics is carried out; extensive simulations show that the common mode defines the shape of a transient frequency swing under relatively small disturbances. The newly derived control strategy pursues a decoupling of the damping control actions at different sites. The concept of modal decomposition control is revisited in the context of static feedback control, it is demonstrated that the distributed static feedback controllers that exclusively add damping to the same mode can be simply superimposed. This means that the control actions can be decoupled by using the sole modal oscillation signals as the input signals of the controllers. Moreover, by properly choosing control sites (areas), the decoupling feature may be retained for the control of multiple modes. With the proposed control strategy, the active power modulations can be flexibly engineered to efficiently utilize the limited power reserve of the supporting devices to mitigate the concerned mode of oscillation; the power response of each device tends to be smaller as more devices are engaged, thereby relieving the concern about the availability of the devices. The linear quadratic regulator based sparsity-promoting (LQRSP) technique is formalized as a tool for determining the least number of system state variables that need to be combined for filtering out the desired sole modal oscillation signals. Extensive studies show that these states are the frequencies scattered in the system. In the proposed framework,

the power command signal for the primary frequency control is determined in a (near) optimal control sense; experiments show that this signal tends to be the system speed seen by the power injection point. Moreover, the decoupled modulating control can effectively isolate the control actions for the inter-area oscillations and the transient frequency swing, thereby greatly relieving the concern about the interaction between the control of these two types of dynamics. Illustrative examples show that the proposed method has advantages over the traditional method in terms of its efficiency in damping of key tie-line power oscillations so as to relieve the reliability concern brought about by a particular power exchange between balancing areas.

With the proposed control method, the research gaps are filled. It is now possible to leverage the huge active power modulation capability of the DERs to enhance the overall stability of the power system with respect to critical frequency oscillations more specifically. Therefore, significantly increase the grid hosting capability of inertia-less DERs.

APPENDIX

Uniqueness of the Proposed Control Method

In general, damping control is not only a pole placement problem; it may need to consider for example the input constraints and robustness to disturbance and even model uncertainty. Movement of the poles on the complex plane with strong modal interactions may need to be avoided. A single standard LQR (multi-mode controller) it is likely to face modal interactions unless the control locations are carefully/luckily selected. This appears to be a poor choice for the DER-based damping control as its location and modulation capacity are determined by many factors. This kind of interaction is common and may be devastating, and when such interaction exists the solution is likely to be compromised. When explicit input constraints are taken into consideration for disturbances at different locations, the 'dynamic modal interaction' may be very different and handling this problem with traditional control design is difficult; when all disturbance locations and all (different) limits are considered, obtaining the solution through existing optimization techniques may be challenging. For DER-based control, the input constraints should be explicitly considered. In references [32, 41, 45], the system is identified and controlled by covering all areas; this ensures robustness of the control system to disturbances. The proposed control approach does not require 'true' wide-area coverage by the actuators, and the decoupled multi-mode control has the potential to overcome the difficulty of controlling closely spaced modes. The strategy is implemented with an LQR approach, thereby endowing good robustness to the control system (e.g., against communication delay, noise, etc.). The control also shows some robustness to changing resource mix.

A Significant Limitation of the Proposed Control Method

The transient frequency swing is triggered by the sudden generation/load imbalance; the system will certainly undergo a strong non-linear process as the power flows need to be redistributed. If the frequency swing is very large, which is the case when considerable change in the power injection occurs somewhere in the system, the step response of a linear

system that mimics the frequency excursion may have non-trivial errors. For a serious contingency that significantly alters the system configuration, a special protection system (SPS) would take responsibility.

A Limitation of the Validation Method

In this dissertation, the proposed control method is validated using a transient stability simulation software. The power injection device model is simplified and the injection interface is ideal. In the future, electromagnetic transient (EMT) simulation with more detailed models is necessary for the further investigations in this field. It is important to examine the interactions between the modulating control actions and the dynamics of the supporting device and the nearby system components. Advanced simulation techniques that can simulate a power system with large-scale power electronics may be desired; however, it is very challenging.

BIBLIOGRAPHY

[1] H. V. Pico, J.D. McCalley, A. Angel, R.Leon, N.J. Castrillon, "Analysis of Very Low Frequency Oscillations in Hydro-Dominant Power Systems Using Multi-Unit Modeling," *IEEE Trans. Power Syst*., vol. 27, no. 4, pp. 1906-1915, Nov. 2012.

[2] G. Tao-Rong, W. Guan-Hong, and L. Tao, "Analysis and control on ultra low frequency oscillation at sending end of UHVDC power system," in *Proc. Int. Conf. IEEE Power System Technol*., 2014, pp. 832–837.

[3] L. Chen, X. Lu, and Y. Min, *et al*, "Optimization of governor parameters to prevent frequency oscillations in power systems," *IEEE Trans. Power Syst*," to be published, 2017.

[4] F. R. Schleif, A. B. Wilbor, "The Coordination of Hydraulic Turbine Governors for Power System Operation," *IEEE Trans. Power App. Syst*., vol. 85, no. 7, pp. 750-758, July 1966.

[5] P. Dandeno, P. Kundur, and J. Bayne, "Hydraulic unit dynamic performance under normal and islanding conditions—analysis and validation," *IEEE Trans. Power App. Syst*., vol. PAS-97, no. 6, pp. 2134–2143, Nov. 1978.

[6] P. Kundur, D. Lee, J. Bayne, and P. Dandeno, "Impact of turbine generator overspeed controls on unit performance under system disturbance conditions," *IEEE Trans. Power App. Syst*., vol. PAS-104, no. 6, pp. 1262–1269, Jun. 1985.

[7] IEEE standard 1207-2011: *Guide for the Application of Turbine Governing Systems for Hydroelectric Generating Units*, IEEE Power and Energy Society

[8] R. Grondin, I. Kamwa, and L. Soulieres, *et al*, "An approach to PSS design for transient stability improvement through supplementary damping of the common low-frequency," *IEEE Trans. Power Syst*., vol. 8, no. 3, pp. 954–963, Aug. 1993.

[9] F. Wilches-Bernal, J. Chow, S. Sanchez-Gasca, "Fundamental Study of Applying Wind Turbines for Power System Frequency Control," *IEEE Trans. Power Syst*., vol. 31, no. 2, pp. 1496 - 1505, March 2016.

[10] D. Rimorov, I. Kamwa, G. Joós, "Quasi-steady-state approach for analysis of frequency oscillations and damping controller design," *IEEE Trans. Power Syst*., vol. 31, no. 4, pp. 3212–3220, Jul. 2016.

[11] A. Moeini, I. Kamwa, "Analytical concepts for reactive power based primary frequency control in power systems," *IEEE Trans. Power Syst*, vol. 31, no. 6, pp. 4217-4230, Nov. 2016.

[12] S. Guggilam, C. Zhao, and E. Dall'Anese, *et al*, "Optimizing DER participation in inertial and primary frequency response," *IEEE Trans. Power Syst*, to be published, 2018.

[13] D. Rimorov, A. Heniche, and I. Kamwa, *et al*, "Dynamic performance improvement of New York state power grid with multi-functional multi-band power system stabilizer-based wide-area control," *IET Gener., Transm. Distrib*, vol. 11, no. 18, pp. 4537-4545, 2017.

[14] P. Kundur, J. Paserba, V. Ajjarapu, G. Andersson, A. Bose, *et al.*, "Definition and classification of power system stability IEEE/CIGRE joint task force on stability terms and definitions," *IEEE Trans. Power Syst*., vol. 19, no. 3, pp. 1387-1401, Aug. 2004.

[15] I. Kamwa, D. Lefebvre, L. Loud, "Small signal analysis of hydro-turbine governors in large interconnected power plants," *Proc. 2002 IEEE Power Engineering Society Winter Meeting*, vol.2, pp. 178 – 1183.

[16] NERC Frequency Response Initiative Report: The Reliability Role of Frequency Response, Oct. 30, 2012, 212p. [Online]. Available: http://www.nerc.com/docs/pc/FRI_Report_10-30-12_Master_w-appendices.pdf

[17] P. M. Anderson, M. Mirheydar, "A low-order system frequency response model," *IEEE Trans. Power Syst*., vol. 5, pp. 720–729, Aug. 1990.

[18] H. Huang, F. Li, "Sensitivity analysis of load-damping characteristic in power system frequency regulation," *IEEE Trans. Power Syst*., vol. 28, no. 2, pp. 1324–1335, May. 2013.

[19] Q. Shi, F. Li, and H. Cui, "An analytical approach to aggregate multi-machine SFR model with applications in power system dynamic studies," *IEEE Trans. Power Syst*, to be published, 2018.

[20] D. J. Trudnowski, "Estimating electromechanical mode shape from synchrophasor measurements," *IEEE Trans. Power Syst*., vol. 23, no. 3, pp. 1188–1195, Aug. 2008.

[21] L. Dosiek, N. Zhou, J. W. Pierre, Z. Huang, and D. J. Trudnowski, "Mode shape estimation algorithms under ambient conditions: A comparative review," *IEEE Trans. Power Syst*., vol. 28, no. 2, pp. 779–787, May 2013.

[22] J. H. Chow, K. W. Cheung, "A toolbox for power system dynamics and control engineering education and research," *IEEE Trans. Power Syst*., vol. 7, no. 4, pp. 1559–1564, Nov. 1992.

[23] P. Kundur, Power System Stability and Control. New York, NY, USA: McGraw-Hill, 1994.

[24] L. Chen, Y. Min, Y. P. Chen, and W. Hu, "Evaluation of generator damping using oscillation energy dissipation and the connection with modal analysis," *IEEE Trans. Power Syst*., vol. 29, no. 3, pp. 1393–1402, May 2014.

[25] R. Xie, D. Trudnowski, "Tracking the damping contribution of a power system component under ambient conditions," *IEEE Trans. Power Syst*., vol. 33, no. 1, pp. 1116–1117, Jan. 2018.

[26] J. C. Mantzaris, A. Metsiou, and C. D. Vournas, "Analysis of interarea oscillations including governor effects and stabilizer design in southeastern Europe," *IEEE Trans. Power Syst*., vol. 28, no. 4, pp. 4948–4956, Nov. 2013.

[27] C. Gencoglu, O. B. Tor, E. Cebeci, O. Yilmaz, A.N. Guven,"Assessment of the effect of hydroelectric power plants' governor settings on low frequency inter area oscillations", 2010 Int. Conf. on Power System Technology (POWERCON), 24-28 Oct. 2010, Hangzhou, China

[28] J. Bendat and A. Presol, *Engineering Applications of Correlation and Spectral Analysis*, 2nd ed. New York, NY, USA: Wiley, 1993.

[29] C. Roberts, *Review of International Grid Codes*, Lawrence Berkeley National Laboratory, Report no. LBNL-2001104, March 2018: https://certs.lbl.gov/sites/default/files/international_grid_codes_lbnl-2001104.pdf

[30] http://www.eps.ee.kth.se/personal/vanfretti/pst/Power_System_Toolbox_Webpage/PST.html

[31] C. Y. Chung, L. Wang, F. Howell, and P. Kundur, "Generation rescheduling methods to improve power transfer capability constrained by small-signal stability," *IEEE Trans. Power Syst.*, vol. 19, no. 1, pp. 524–530, Feb. 2004.

[32] I. Kamwa, R. Grondin, and Y. Hebert, "Wide-area measurement-based stabilizing control of large power systems—A decentralized/hierarchical approach," *IEEE Trans. Power Syst.*, vol. 16, no. 1, pp. 136–153, Feb. 2001.

[33] B. Chaudhuri and B. C. Pal, "Robust damping of multiple swing modes employing global stabilizing signals with a TCSC*," IEEE Trans. Power Syst*., vol. 19, no. 1, pp. 499–506, Feb. 2004.

[34] L. Chen, Y. Min, and X. M. Lu, *et al*., "Online emergency control to suppress frequency oscillations based on damping evaluation using dissipation energy flow," *International Journal of Electrical Power and Energy Systems*, vol. 103, pp. 414–420, Dec. 2018.

[35] B. J. Pierre, F. Wilches-Bernal, D. A. Schoenwald, R. T. Elliott, D. J. Trudnowski, R. H. Byrne, and J. C. Neely, "Design of the Pacific DC Intertie wide area damping controller," *IEEE Trans. Power Syst*., vol. 34, no. 5, pp. 3594–3604, Sep. 2019.

[36] C. Lu, X. C. Wu, J. T. Wu, P. Li, Y. D. Han, and L. C. Li, "Implementations and experiences of wide-area HVDC damping control in China southern power grid," in Proc. IEEE Power Energy Soc. General Meeting, July 2012, pp. 1–7.

[37] B. K. Poolla, D. Gross, and F. Dörfler, "Placement and implementation of grid-forming and grid-following virtual inertia and fast frequency response," *IEEE Trans. Power Syst*., vol. 34, no. 4, pp. 3035–3046, Jul. 2019.

[38] Y. L. Zhu, C. X. Liu, K. Sun, D. Shi, and Z. W. Wang, ''Optimization of battery energy storage to improve power system oscillation damping,'' *IEEE Trans. Sustain. Energy*, vol. 10, no. 3, pp. 1015–1024, Jul. 2019.

[39] A. Delavari and I. Kamwa, "Improved optimal decentralized load modulation for power system primary frequency regulation," *IEEE Trans. Power Syst*., vol. 33, no. 1, pp. 1013–1025, Jan. 2018.

[40] F. Wilches-Bernal, D. A. Copp, G. Bacelli, and R. H. Byrne, “Structuring the optimal output feedback control gain: a soft constraint approach,” 2018 IEEE Conference on Decision and Control (CDC).

[41] F. Wilches-Bernal, R. H. Byrne, and J. M. Lian, “Damping of inter-area oscillations via modulation of aggregated loads,” *IEEE Trans. Power Syst.*, vol. 35, no. 3, pp. 2024–2036, May. 2020.

[42] J. B. Zhang, C. Y. Chung, and Y. D. Han, “A novel modal decomposition control and its application to PSS design for damping inter-area oscillations in power systems,” *IEEE Trans. Power Syst.*, vol. 27, no. 4, pp. 2015–2025, Nov. 2012.

[43] J. B. Zhao *et al.*, “Power system dynamic state estimation: Motivations, definitions, methodologies and future work,” *IEEE Trans. Power Syst.*, vol. 34, no. 4, pp. 3188–3198, Jul. 2019.

[44] F. Lin, M. Fardad, and M. R. Jovanović, “Design of optimal sparse feedback gains via the alternating direction method of multipliers,” *IEEE Trans. Automat. Control*, vol. 58, no. 9, pp. 2426–2431, Sep. 2013.

[45] F. Dörfler, M. R. Jovanović, M. Chertkov, and F. Bullo, “Sparsity-promoting optimal wide-area control of power networks,” *IEEE Trans. Power Syst.*, vol. 29, no. 5, pp. 2281–2291, Sep. 2014.

[46] X. F. Wu, F. Dörfler, and M. R. Jovanović, “Input-output analysis and decentralized optimal control of inter-area oscillations in power systems,” *IEEE Trans. Power Syst.*, vol. 31, no. 3, pp. 2434–2444, May 2016.

[47] R. C. Xie, I. Kamwa, D. Rimorov, and A. Moeini, "Fundamental study of common mode small-signal frequency oscillations in power systems," *International Journal of Electrical Power and Energy Systems*, vol. 106, pp. 201–209, Mar. 2019.

[48] R. L. Cresap, W. A. Mittelstadt, D. N. Scott, and C. W. Taylor, “Operating experience with modulation of the Pacific HVDC Intertie,” IEEE Trans. on Power Apparatus and Systems, vol. PAS-97, no. 4, pp. 1053-1059, July/Aug. 1978.

[49] I. Kamwa, R. Grondin, D. Asber, J.P. Gingras, “Active-power stabilizers for multimachine power systems: challenges and prospects,” Paper PE-906-PWRS-0-10-1997, to appear in IEEE Trans. Power Syst., 1998.

[50] I. Kamwa, R. Grondin, D. Asber, J. P. Gingras, and G. Trudel, “Large-scale active load modulation for angle stability improvement,” IEEE Trans., vol. PWRS-14, no. 2, pp. 582–590, May 1999.

[51] D. J. Trudnowski, J. R. Smith, T. A. Short, and D. A. Pierre, “An application of Prony methods in PSS design for multi-machine systems,” *IEEE Trans. Power Syst.*, vol. 6, no. 1, pp. 118–126, Feb. 1991.

[52] Y. Zhang and A. Bose, “Design of wide-area damping controllers for interarea oscillations,” *IEEE Trans. Power Syst.*, vol. 23, no. 3, pp. 1136– 1143, Aug. 2008.

[53] M. Klein, L. Le, G. Rogers, S. Farrokpay, and N. Balu, “H damping controller design in large power system,” *IEEE Trans. Power Syst.*, vol. 10, pp. 158–166, Feb. 1995

[54] G. Taranto and J. Chow, “A robust frequency domain optimization technique for tuning series compensation damping controllers,” *IEEE Trans. Power Syst*., vol. 10, pp. 1219–1225, Aug. 1995.

[55] B. Pal, A. Coonick, I. Jaimoukha, and H. Zobaidi, “A linear matrix inequality approach to robust damping control design in power systems with superconducting magnetic energy storage device,” *IEEE Trans. Power Syst*., vol. 15, pp. 356–362, Feb. 2000.

[56] S. Obuz, M. Ayar, R. D. Trevizan, C. Ruben, and A. S. Bretas, ‘‘Renewable and energy storage resources for enhancing transient stability margins: A PDE-based nonlinear control strategy,’’ *International Journal of Electrical Power and Energy Systems*, vol. 116, Mar. 2020, Art. no. 105510.

[57] S. J. Hossain, R. Bhattarai, R. Yousefian, and S. Kamalasadan, ‘‘Adaptive wide area damping controller for distributed energy resources integrated power grid,’’ in Proc. IEEE Power Energy Soc. Gen. Meeting (PESGM), Aug. 2018, pp. 1–5.

[58] T. Sadamoto, A. Chakrabortty, T. Ishizaki, and J. Imura, “Dynamic modeling, stability, and control of power systems with distributed energy resources: Handling faults using two control methods in tandem,” IEEE Control Syst. Mag., vol. 39, no. 2, pp. 34–65, Apr. 2019.

[59] Sasahara, H., Ishizaki, T., Sadamoto, T., Masuta, T., Ueda, Y., Sugihara, H., Yamaguchi, N., and Imura, J.-i., 2019, "Damping performance improvement for PV-integrated power grids via retrofit control," *Control Engineering Practice*, 84, pp. 92-101.

[60] D. Wang, M. Glavic, and L. Wehenkel, “Comparison of centralized, distributed and hierarchical model predictive control schemes for electromechanical oscillations damping in large-scale power systems,” *International Journal of Electrical Power and Energy Systems*, vol. 58, pp. 32–41, Jun. 2014.

[61] N. Hatziargyriou, J. Milanovic, C. Rahmann, V. Ajjarapu, C. Cañizares, I. Erlich, D. Hill, I. Hiskens, I. Kamwa, B. Pal, and P. Pourbeik, ‘‘Stability definitions and characterization of dynamic behavior in systems with high penetration of power electronic interfaced technologies,’’ IEEE, Piscataway, NJ, USA, Tech. Rep. PES-TR77, Apr. 2020.

[62] Y. Chompoobutrgool, L. Vanfretti, and M. Ghandhari, “Survey on power system stabilizers control and their prospective applications for power system damping using synchrophasor-based wide-area systems,” *Eur. Trans. Elect. Power*, vol. 21, no. 8, pp. 2098–2111, 2011.

[63] X. R. Zhang, C. Lu, S. C. Liu, and X. Y. Wang, “A review on widearea damping control to restrain inter-area low frequency oscillation for large-scale power systems with increasing renewable generation,” *Renew. Sustain. Energy Rev*., vol. 57, pp. 45–48, May 2016.

[64] R. Majumder, B. Chaudhuri, and B.C. Pal, "A probabilistic approach to model-based adaptive control for damping of interarea oscillations," *IEEE Trans. Power Syst.,* vol. 20, no. 1, pp. 367-374, Feb. 2005.

[65] L. Zhou, X. Yu, B. Li *et al.*, "Damping inter-area oscillations with large-scale PV plant by modified multiple-model adaptive control strategy," *IEEE Trans. Sustain. Energy,* vol. 8, no. 4, pp. 1629-1636, Oct. 2017.

[66] J. Ma, T. Wang, Z. Wang, and J. S. Thorp, "Adaptive damping control of inter-area oscillations based on federated Kalman filter using wide area signals," *IEEE Trans. Power Syst.,* vol. 28, no. 2, pp. 1627-1635, May 2013.

[67] F. Milano, F. Dorfler, G. Hug, D. Hill, and G. Verbic, “Foundations and ¨ challenges of low-inertia systems,” in Proc. Power Syst. Comput. Conf., 2018.

[68] A. Delavari and I. Kamwa, “Virtual inertia-based load modulation for power system primary frequency regulation,” in Proc. IEEE Power Energy Soc. General Meeting, Chicago, IL USA, to be published, Jul. 16-20, 2017.

[69] A. Delavari and I. Kamwa, ‘‘Sparse and resilient hierarchical direct load control for primary frequency response improvement and inter-area oscillations damping,’’ *IEEE Trans. Power Syst*., vol. 33, no. 5, pp. 5309–5318, Sep. 2018.

[70] https://naspi.org/node/749.

[71] S. Boyd, N. Parikh, E. Chu, B. Peleato, and J. Eckstein, “Distributed optimization and statistical learning via the alternating direction method of multipliers,” Found. Trends Mach. Learning, vol. 3, no. 1, pp. 1–124, 2011.